Inorganic Chemistry

Article

pubs.acs.org/IC

Intraligand Charge-Transfer Excited States in Re(I) Complexes with Donor-Substituted Dipyridophenazine Ligands

Christopher B. Larsen,[†] Holly van der Salm,[†] Charlotte A. Clark,[‡] Anastasia B. S. Elliott,[†] Michael G. Fraser,[†] Raphael Horvath,[‡] Nigel T. Lucas,[†] Xue-Zhong Sun,[‡] Michael W. George,*[,‡] and Keith C. Gordon*[,†]

[†]MacDiarmid Institute for Advanced Materials and Nanotechnology, Department of Chemistry, University of Otago, Union Place, Dunedin 9001, New Zealand

[‡]School of Chemistry, University of Nottingham, University Park, Nottingham NG7 2RD, United Kingdom

Supporting Information

ABSTRACT: The donor−acceptor ligands 11-(4-diphenylaminophenyl)dipyrido[3,2-*a*:2′,3′-*c*]phenazine (dppz-PhNPh$_2$) and 11-(4-dimethylaminophenyl)dipyrido[3,2-*a*:2′,3′-*c*]-phenazine (dppz-PhNMe$_2$), and their rhenium complexes, [Re(CO)$_3$X] (X = Cl$^-$, py, 4-dimethylaminopyridine (dmap)), are reported. Crystal structures of the two ligands were obtained. The optical properties of the ligands and complexes are dominated by intraligand charge transfer (ILCT) transitions from the amine to the dppz moieties with λ_{abs} = 463 nm (ε = 13 100 M^{-1} cm^{-1}) for dppz-PhNMe$_2$ and with λ_{abs} = 457 nm (ε = 16 900 M^{-1} cm^{-1}) for dppz-PhNPh$_2$. This assignment is supported by CAM-B3LYP TD-DFT calculations. These ligands are strongly emissive in organic solvents and, consistent with the ILCT character, show strong solvatochromic behavior. Lippert−Mataga plots of the data are linear and yield $\Delta\mu$ values of 22 D for dppz-PhNPh$_2$ and 20 D for dppz-PhNMe$_2$. The rhenium(I) complexes are less emissive, and it is possible to measure resonance Raman spectra. These data show relative band intensities that are virtually unchanged from λ_{exc} = 351 to 532 nm, consistent with a single dominant transition in the visible region. Resonance Raman excitation profiles are solvent sensitive; these data are modeled using wavepacket theory yielding reorganization energies ranging from 1800 cm^{-1} in toluene to 6900 cm^{-1} in CH$_3$CN. The excited state electronic absorption and infrared spectroscopy reveal the presence of dark excited states with nanosecond to microsecond lifetimes that are sensitive to the ancillary ligand on the rhenium. These dark states were assigned as phenazine-based ^{3}ILCT states by time-resolved infrared spectroscopy. Time-resolved infrared spectroscopy shows transient features in which $\Delta\nu$(CO) is approximately −7 cm^{-1}, consistent with a ligand-centered excited state. Evidence for two such states is seen in mid-infrared transient spectra.

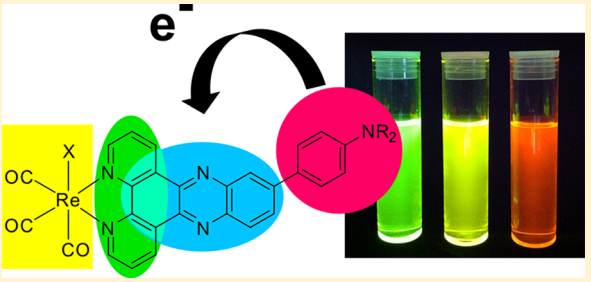

INTRODUCTION

Dipyridophenazine (dppz) based ligands and their complexes have been extensively studied due to their interesting photophysical properties.[1−6] These are derived from the presence of two close-lying acceptor molecular orbitals (MOs) that lie on different sections of the ligand.[7−10] In dppz-based systems the b$_1$(phen) orbital has wave function amplitude localized on the phenanthroline portion of the ligand (rings A, B, and C in Figure 1), while the b$_1$(phz) orbital has electron density localized on the phenazine portion of the ligand (rings B, D, and E in Figure 1).[4]

The most well-known manifestation of these two acceptor orbitals is the phenomenon known as the "light-switch" effect, in which [Ru(bpy)$_2$(dppz)]$^{2+}$ is nonemissive in protic media, but emissive in aprotic media or in the presence of double-stranded DNA.[11−17] This effect occurs because the b$_1$(phz) metal to ligand charge transfer (MLCT) state is nonemissive and the b$_1$(phen) MLCT state emissive.[4] The "light-switch" behavior was originally attributed to protonation of the phz nitrogen atoms stabilizing the nonemissive b$_1$(phz) state in aqueous media.[18] Brennaman et al.,[19] based on variable temperature lifetime studies, further developed this model in proposing that the dark b$_1$(phz) state is always the lowest energy state, even in aprotic solvents, and that the "light-switch" is driven by competition between enthalpic factors that favor the dark b$_1$(phz) state and entropic factors that favor the emissive b$_1$(phen) state.

Research in this area has focused on manipulating the relative energies of the two MOs. This may be achieved by chelation to various metals[20−26] which alters the b$_1$(phen) MO. Substitution at the dppz ligand has mostly involved lowering the energy of the b$_1$(phz) state through appending electron-withdrawing groups to the E ring.[20,27−34] In addition, in one study the

Received: August 15, 2013
Published: January 21, 2014

   dx.doi.org/10.1021/ic402082m | Inorg. Chem. 2014, 53, 1339−1354

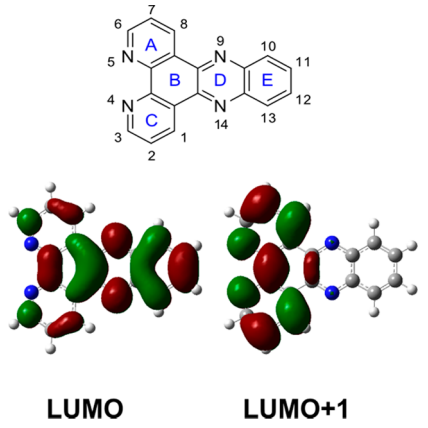

Figure 1. Dppz ligand structure with ring labels and numbering, and phenazine (phz) LUMO and phenanthroline (phen) LUMO + 1.

energy of the b_1(phen) state was modified through substitution at the A and C rings.[20] Recent studies have used dppz as an acceptor motif, connected to sulfur-based donors.[27,30,35−40] Jia et al. demonstrated a tetrathiafulvalene (TTF)−dppz donor−acceptor (D−A) couple with a change in dipole moment of 16 D.[38] Goze et al. then demonstrated the same ligand as a series of ruthenium complexes: $[Ru(bpy)_2(dppz\text{-}TTF)]^{2+}$, $[Ru(bpy)(dppz\text{-}TTF)_2]^{2+}$, and $[Ru(dppz\text{-}TTF)_3]^{2+}$.[37] They proposed that initial excitation could occur as either ^{1}ILCT or ^{1}MLCT transitions, and that the ^{1}MLCT could undergo an electron-transfer process with a neighboring ligand (either bpy or dppz-TTF, depending on the complex) to do one of three things: form a ligand−ligand charge-separated (LLCS) state, intersystem cross to a ^{3}MLCT state, or undergo an electron-transfer event with the TTF of the same ligand to form the ^{1}ILCT state. Both the ^{1}ILCT and ^{3}MLCT states are emissive, consistent with the dual emission observed.

These complexes showed isolated ILCT and MLCT transitions, whereas the $\{Re(CO)_3Cl\}$ and $\{Cu(bpy)\}^+$ dppz complexes with appended sulfur-based donors reported by Fraser et al. show a charge-transfer event that has a combination of MLCT and ILCT character.[40,41] The donation of electron density from the metal and sulfur-based donor into the dppz manifests as an absorption band that is much more intense than the sum of the MLCT and ILCT transitions.

In an attempt to further understand the properties of Re(I) dppz complexes with appended donor groups, we have synthesized two dppz ligands with amine donors, dppz-$PhNPh_2$ and dppz-$PhNMe_2$ and their $\{Re(CO)_3X\}$ (X = Cl, pyridine and dimethylaminopyridine (dmap)) complexes (Figure 2). This is the first study to investigate amine-substituted donor−acceptor Redppz systems although the use of triarylamine-based donor groups has been heavily investigated in a range of donor−acceptor studies and for use in photovoltaic dyes.[42−55]

The electronic donor−acceptor behavior of these compounds has been characterized by B3LYP and CAM-B3LYP TD-DFT calculations (validated by FT-Raman spectroscopy and X-ray crystallography), cyclic voltammetry, and variable temperature and variable solvent steady state absorption and emission, transient absorption, and resonance Raman spectroscopies. We observe an intense ILCT transition in all of the studied compounds, as well as an interplay between dark and emissive excited states that may be modulated by the ancillary ligands of the rhenium.

EXPERIMENTAL SECTION

Materials. Commercially available reagents were used as received. Literature procedures were used to prepare 1,10-phenanthroline-5,6-dione[56] and 11-bromodipyrido[3,2-*a*:2′,3′-*c*]phenazine.[32] Rhenium complexes were synthesized by previously reported methods.[23,34,57]

General Procedure for the Preparation of dppz Ligands dppz-$PhNPh_2$ and dppz-$PhNMe_2$. To a deoxygenated mixture of 11-bromodipyrido[3,2-*a*:2′,3′-*c*]phenazine (∼1.5 mmol), boronic acid (∼3.1 mmol), and K_2CO_3 (∼15 mmol) in toluene (50 mL), water (20 mL), and EtOH (10 mL) was added dichloro[1,1′-bis-(diphenylphosphino)ferrocene]palladium(II) (∼0.15 mmol). The reaction mixture was heated at reflux under an Ar atmosphere overnight and cooled and the volatiles removed under reduced pressure. The reaction material was washed with copious amounts of water and CH_3CN. The crude product was purified by preparative column chromatography ($CHCl_3$, Al_2O_3) and recrystallized by hexane diffusion into a $CHCl_3$ solution.

11-(4-Diphenylaminophenyl)dipyrido[3,2-a:2′,3′-c]phenazine (dppz-$PhNPh_2$). Following the general procedure with 11-bromodipyrido[3,2-*a*:2′,3′-*c*]phenazine (0.504 g, 1.40 mmol), 4-(diphenylaminophenyl)boronic acid (0.517 g, 1.79 mmol), K_2CO_3 (2.07 g, 14.9 mmol), and dichloro[1,1′-bis(diphenylphosphino)-ferrocene]palladium(II) (0.177 g, 0.216 mmol), dppz-$PhNPh_2$ was isolated (0.696 g, 74%) as an orange crystalline solid. ^{1}H NMR ($CDCl_3$, 500 MHz): δ 9.64 (m, 2H, $H_{1,8}$), 9.28 (td, J = 1.6, 4.4 Hz, 2H, $H_{3,6}$), 8.50 (d, J = 1.9 Hz, 1H, H_{10}), 8.37 (d, J = 8.8 Hz, 1H, H_{12}), 8.20 (dd, J = 2.1, 8.9 Hz, 1H, H_{13}), 7.80 (dd, J = 7.9, 4.2 Hz, 2H, $H_{2,7}$), 7.75 (d, J = 8.7 Hz, 2H, H_{Ph}), 7.33 (t, J = 8.5 Hz, 4H, N*Ph*$_2$), 7.24 (d, J = 8.7 Hz, 2H, *Ph*), 7.20 (dd, J = 8.5, 1.1 Hz, 4H, N*Ph*$_2$), 7.10 (tt, J = 8.5, 1.2 Hz, 2H, N*Ph*$_2$) ppm. ^{13}C NMR ($CDCl_3$, 125 MHz): δ 152.6, 152.5, 148.7, 148.0, 147.5, 143.1, 142.9, 142.0, 141.6, 140.7, 134.0, 133.9, 132.6, 130.5, 129.9, 129.6, 129.4, 129.3, 128.4, 127.9, 127.8, 125.5, 125.1, 124.4, 124.3, 123.7, 123.4, 122.18 ppm. HRMS (ESI) Calcd for $C_{36}H_{24}N_5$ ($[M + H]^+$): m/z 526.2026. Found: 526.2035. Anal. Calcd for $C_{36}H_{23}N_5{\cdot}CHCl_3$: C, 68.90; H, 3.75; N, 10.86. Found: C, 69.01; H, 3.71; N, 10.93.

11-(4-Dimethylaminophenyl)dipyrido[3,2-a:2′,3′-c]phenazine (dppz-$PhNMe_2$). Following the general procedure with 11-bromodipyrido[3,2-*a*:2′,3′-*c*]phenazine (0.524 g, 1.45 mmol), 4-(dimethylaminophenyl)boronic acid (0.512 g, 3.10 mmol), K_2CO_3 (2.35 g, 17.0 mmol), and dichloro[1,1′-bis(diphenylphosphino)-ferrocene]palladium(II) (0.133 g, 0.162 mmol), dppz-$PhNMe_2$ was isolated (0.420 g, 72%) as an orange crystalline solid. ^{1}H NMR ($CDCl_3$, 500 MHz): δ 9.67−9.62 (m, 2H, $H_{1,8}$), 9.28−9.25 (m, 2H, $H_{3,6}$), 8.47 (1H, d, J = 2.1 Hz, H_{10}), 8.34 (d, J = 8.9 Hz, 1H, H_{13}), 8.22 (dd, J = 8.9, 2.1 Hz, 1H, H_{12}), 7.81−7.78 (m, 4H, $H_{2,7}$, *Ph*), 6.89 (d, J

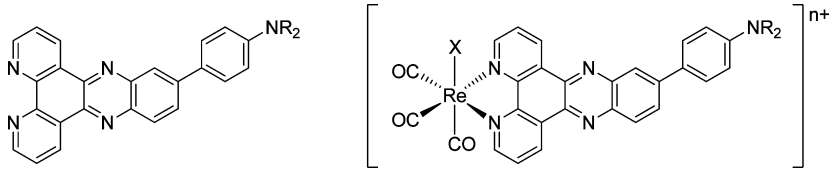

Figure 2. General structure of ligands and Re(I) complexes presented in this Article, where R = Me, Ph and X = Cl, py, dmap. n = 1 when X = py, dmap; n = 0 when X = Cl.

dx.doi.org/10.1021/ic402082m | *Inorg. Chem.* 2014, 53, 1339−1354

= 8.8 Hz, 2H, *Ph*), 3.08 (s, 6H, NMe_2) ppm. ^{13}C NMR ($CDCl_3$, 125 MHz): 152.6, 152.4, 150.9, 148.5, 148.3, 143.5, 143.3, 141.8, 141.5, 140.3, 133.9, 133.7, 130.5, 129.7, 128.4, 128.0, 127.9, 124.2, 124.2, 112.9, 40.6 ppm. HRMS (ESI) calcd for $C_{26}H_{20}N_5$ ($[M+H]^+$): *m*/*z* 402.1713; found: 402.1715. Elemental analysis calcd for $C_{26}H_{19}N_5 \cdot CHCl_3$: C, 62.26; H, 3.87; N, 13.45. Found: C, 62.18; H, 3.67; N, 13.63.

General procedure for the preparation of [$ReCl(CO)_3$(dppz-$PhNPh_2$)] and [$ReCl(CO)_3$(dppz-$PhNMe_2$)]. A mixture of dppz ligand (~0.6 mmol) and pentacarbonylrhenium(I) chloride (~0.7 mmol) in EtOH (100 mL) was heated at reflux overnight. The reaction mixture was allowed to cool, filtered and the precipitate washed with EtOH.

fac-Chlorotricarbonyl(11-(4-diphenylaminophenyl)dipyrido[3,2-a:2′,3′-c]phenazine)rhenium(I), [$ReCl(CO)_3$(dppz-$PhNPh_2$)]. Following the general procedure with 11-(4-diphenylaminophenyl)dipyrido-[3,2-*a*:2′,3′-*c*]phenazine (0.298 g, 0.568 mmol) and pentacarbonylrhenium(I) chloride (0.272 g, 0.751 mmol), [$ReCl(CO)_3$(dppz-$PhNPh_2$)] was isolated (0.429 g, 91%) as a black solid. ^1H NMR ($CDCl_3$, 400 MHz): δ 9.86 (t, *J* = 7.5 Hz, 2H), 9.45 (t, *J* = 5.0 Hz, 2H), 8.57 (s, 1H), 8.46 (d, *J* = 9.0 Hz, 1H), 8.33 (d, *J* = 9.3 Hz, 1H), 8.04–8.00 (m, 2H), 7.77 (d, *J* = 8.5 Hz, 2H), 7.34 (t, *J* = 7.6 Hz, 4H), 7.23–7.20 (m, 6H), 7.12 (t, *J* = 7.5 Hz, 2H) ppm. HRMS (ESI) calcd for $C_{39}H_{23}ClN_5NaO_3Re$ ($[M+Na]^+$): *m*/*z* 854.0939; found: 854.0810. Elemental analysis calcd. for $C_{39}H_{23}ClN_5O_3Re \cdot H_2O$: C, 55.15; H, 2.97; N, 8.25. Found: C, 54.89; H, 3.01; N, 8.23.

fac-Chlorotricarbonyl(11-(4-dimethylaminophenyl)dipyrido[3,2-a:2′,3′-c]phenazine)rhenium(I), [$ReCl(CO)_3$(dppz-$PhNMe_2$)]. Following the general procedure with 11-(4-dimethylaminophenyl)dipyrido-[3,2-*a*:2′,3′-*c*]phenazine (0.251 g, 0.624 mmol) and pentacarbonylrhenium(I) chloride (0.258 g, 0.712 mmol), [$ReCl(CO)_3$(dppz-$PhNMe_2$)] was isolated (0.370 g, 84%) as a dark purple solid. ^1H NMR ($CDCl_3$, 400 MHz): δ 9.87–9.82 (m, 2H), 9.46–9.43 (m, 2H), 8.53 (s, 1H), 8.42 (d, *J* = 8.9 Hz, 1H), 8.35 (d, *J* = 9.0 Hz, 1H), 8.03–7.99 (m, 2H), 7.85 (d, *J* = 8.4 Hz, 2H), 7.05–6.91 (m, 2H), 3.14 (s, 6H) ppm. HRMS (ESI) Calcd for $C_{29}H_{21}N_5O_4Re$ ($[M - Cl + H_2O]^+$): *m*/*z* 690.1146. Found: 690.1107. Anal. Calcd for $C_{29}H_{19}ClN_5O_3Re$: C, 49.26; H, 2.71; N, 9.90. Found: C, 49.27; H, 2.69; N, 9.96.

General Procedure for the Preparation of [$Re(CO)_3$(dppz-$PhNPh_2$)(CH_3CN)]PF_6 and [$Re(CO)_3$(dppz-$PhNMe_2$)(CH_3CN)]PF_6. A mixture of rhenium complex (~0.3 mmol) and AgOTf (~1 mmol) in CH_3CN (100 mL) was heated at reflux under an Ar atmosphere overnight. The reaction was allowed to cool, and then filtered through Celite. To the reaction was added aqueous NH_4PF_6 (~1.8 mmol), and the reaction was concentrated under reduced pressure. The crude product was washed with water, and then characterized by ^1H NMR spectroscopy and reacted without further purification or further characterization.

fac-Acetonitriletricarbonyl(11-(4-diphenylaminophenyl)dipyrido-[3,2-a:2′,3′-c]phenazine)rhenium(I) Hexafluorophosphate, [Re-($CO)_3$(dppz-$PhNPh_2$)(CH_3CN)]PF_6. Following the general procedure with *fac*-chlorotricarbonyl(11-(4-diphenylaminophenyl)dipyrido[3,2-*a*:2′,3′-*c*]phenazine)rhenium(I) (0.232 g, 0.278 mmol), AgOTf (0.239 g, 0.932 mmol), and NH_4PF_6 (0.300 g, 1.84 mmol), [$Re(CO)_3$(dppz-$PhNPh_2$)(CH_3CN)]PF_6 was isolated (0.249 g, 91%) as a purple solid. ^1H NMR ($CDCl_3$, 400 MHz): δ 10.02 (t, *J* = 7.5 Hz, 2H), 9.36 (t, *J* = 5.5 Hz, 2H), 8.57 (s, 1H), 8.46 (d, *J* = 9.0 Hz, 1H), 8.32 (d, *J* = 9.0 Hz, 1H), 8.15 – 8.10 (m, 2H), 7.76 (d, *J* = 8.3 Hz, 2H), 7.34 (t, *J* = 7.7 Hz, 4H), 7.26 – 7.20 (m, 6H), 7.12 (t, *J* = 7.7 Hz, 2H), 2.20 (s, 3H) ppm.

fac-Acetonitriletricarbonyl(11-(4-dimethylaminophenyl)dipyrido-[3,2-a:2′,3′-c]phenazine)rhenium(I) Hexafluorophosphate, [Re-($CO)_3$(dppz-$PhNMe_2$)(CH_3CN)]PF_6. Following the general procedure with *fac*-chlorotricarbonyl(11-(4-dimethylaminophenyl)dipyrido[3,2-*a*:2′,3′-*c*]phenazine)rhenium(I) (0.246 g, 0.348 mmol), AgOTf (0.239 g, 0.932 mmol), and NH_4PF_6 (0.300 g, 1.84 mmol), [$Re(CO)_3$(dppz-$PhNMe_2$)(CH_3CN)]PF_6 was isolated (0.257 g, 86%) as a purple solid. ^1H NMR ($(CD_3)_2CO$, 400 MHz): δ 10.06 (m, 2H), 9.71 (m, *J* = 4.6, 8.6 Hz, 2H), 8.60–8.57 (m, 2H), 8.51 (d, *J* = 8.9 Hz, 1H), 8.45 (dd, *J* = 13.0, 7.1 Hz, 2H), 7.96 (d, *J* = 8.5 Hz, 2H), 6.98 (d, *J* = 8.6 Hz, 2H), 3.10 (s, 6H), 2.21 (s, 3H) ppm.

General Procedure for the Preparation of [$Re(CO)_3$(dppz-$PhNPh_2$)(py)]PF_6 and [$Re(CO)_3$(dppz-$PhNMe_2$)(py)]PF_6. A mixture of acetonitrile complex (~0.15 mmol) and pyridine (~3 mmol) in THF (50 mL) was heated at reflux under an Ar atmosphere overnight. The reaction was allowed to cool, and then filtered through Celite. Aqueous NH_4PF_6 (~1.8 mmol) was added and the reaction mixture concentrated under reduced pressure. The crude product was washed with copious amounts of water.

fac-Pyridinetricarbonyl(11-(4-diphenylaminophenyl)dipyrido-[3,2-a:2′,3′-c]phenazine)rhenium(I) Hexafluorophosphate, [Re-($CO)_3$(dppz-$PhNPh_2$)(py)]PF_6. Following the general procedure with *fac*-acetonitriletricarbonyl(11-(4-diphenylaminophenyl)dipyrido[3,2-*a*:2′,3′-*c*]phenazine)rhenium(I) hexafluorophosphate (0.126 g, 0.128 mmol), pyridine (0.3 mL, 3.71 mmol), and NH_4PF_6 (0.300 g, 1.84 mmol), [$Re(CO)_3$(dppz-$PhNPh_2$)(py)]PF_6 was isolated (0.122 g, 93%) as a purple solid. ^1H NMR ($CDCl_3$, 400 MHz): δ 9.98 (t, *J* = 8.8 Hz, 2H), 9.59 (t, *J* = 5.9 Hz, 2H), 8.54 (d, *J* = 1.8 Hz, 1H), 8.42 (d, *J* = 9.0 Hz, 1H), 8.38 (d, *J* = 4.9 Hz, 2H), 8.33–8.30 (m, 3H), 7.74 (d, *J* = 8.6 Hz, 2H), 7.70 (t, *J* = 8.0 Hz, 1H), 7.38–7.33 (m, 2H), 7.33 (t, *J* = 7.9, 4H), 7.21 (t, *J* = 8.5 Hz, 4H), 7.21–7.17 (m, 2H), 7.12 (t, *J* = 7.4 Hz, 2H) ppm. HRMS (ESI) Calcd for $C_{44}H_{28}N_6O_3Re$ ($[M]^+$): *m*/*z* 875.1780. Found: 875.1772. Anal. Calcd for $C_{44}H_{28}F_6N_6O_3PRe \cdot H_2O$: C, 50.92; H, 2.91; N, 8.10. Found: C, 51.06; H, 2.86; N, 8.06.

fac-Pyridinetricarbonyl(11-(4-dimethylaminophenyl)dipyrido-[3,2-a:2′,3′-c]phenazine)rhenium(I) Hexafluorophosphate, [Re-($CO)_3$(dppz-$PhNMe_2$)(py)]PF_6. Following the general procedure with *fac*-acetonitriletricarbonyl(11-(4-dimethylaminophenyl)dipyrido[3,2-*a*:2′,3′-*c*]phenazine)rhenium(I) hexafluorophosphate (0.130 g, 0.151 mmol), pyridine (0.3 mL, 3.71 mmol), and NH_4PF_6 (0.300 g, 1.84 mmol), [$Re(CO)_3$(dppz-$PhNMe_2$)(py)]PF_6 was isolated (0.126 g, 93%) as a purple solid. ^1H NMR ($(CD_3)_2CO$, 400 MHz): δ 10.03 (m, 2H), 9.96 (m, 2H), 8.70 (d, *J* = 5.7 Hz, 2H), 8.55 (s, 1H), 8.53–8.43 (m, 4H), 7.93 (d, *J* = 8.3 Hz, 3H), 7.41 (t, *J* = 6.8 Hz, 2H), 6.96 (d, *J* = 8.4 Hz, 2H), 3.09 (s, 6H) ppm. HRMS (ESI) Calcd for $C_{34}H_{24}N_6O_3Re$ ($[M]^+$): *m*/*z* 751.1467. Found: 751.1495. Anal. Calcd for $C_{34}H_{24}F_6N_6O_3PRe \cdot H_2O$: C, 44.69; H, 2.87; N, 9.20. Found: C, 44.71; H, 2.83; N, 9.10.

General Procedure for the Preparation of [$Re(CO)_3$(dppz-$PhNPh_2$)(dmap)]PF_6 and [$Re(CO)_3$(dppz-$PhNMe_2$)(dmap)]PF_6. A mixture of acetonitrile complex (~0.15 mmol) and 4-dimethylaminopyridine (~3 mmol) in THF (50 mL) was heated at 70 °C under an Ar atmosphere overnight. The reaction was allowed to cool, and then filtered through Celite. Aqueous NH_4PF_6 (~1.8 mmol) was added and the reaction mixture concentrated under reduced pressure. The crude product was washed with copious amounts of water.

fac-(4-Dimethylaminopyridine)tricarbonyl(11-(4-diphenylaminophenyl)dipyrido[3,2-a:2′,3′-c]phenazine)rhenium(I) Hexafluorophosphate, [Re($CO)_3$(dppz-$PhNPh_2$)(dmap)]PF_6. Following the general procedure with *fac*-acetonitriletricarbonyl(11-(4-diphenylaminophenyl)dipyrido[3,2-*a*:2′,3′-*c*]phenazine)rhenium(I) hexafluorophosphate (0.120 g, 0.122 mmol), 4-dimethylaminopyridine (0.372 g, 3.04 mmol), and NH_4PF_6 (0.300 g, 1.84 mmol), [$Re(CO)_3$(dppz-$PhNPh_2$)(dmap)]PF_6 (0.121 g, 93%) was isolated as a purple solid. ^1H NMR ($CDCl_3$, 400 MHz): δ 9.98 (t, *J* = 7.0 Hz, 2H), 9.51 (t, *J* = 4.7 Hz, 2H), 8.55 (s, 1H), 8.43 (d, *J* = 8.9 Hz, 1H), 8.31 (d, *J* = 8.3 Hz, 1H), 8.25 (m, 2H), 7.75 (d, *J* = 8.6 Hz, 2H), 7.67 (m, 2H), 7.34 (t, *J* = 8.1 Hz, 4H) 7.24–7.19 (m, 6H), 7.12 (t, *J* = 7.4 Hz, 2H), 6.34 (m, 2H), 2.84 (s, 6H) ppm. HRMS (ESI) Calcd for $C_{46}H_{33}F_6N_7O_3PRe$ ($[M]^+$): *m*/*z* 918.2202. Found: 918.2184. Anal. Calcd for $C_{46}H_{33}F_6N_7O_3PRe \cdot 2H_2O$: C, 50.27; H, 3.39; N, 8.92. Found: C, 50.61; H, 3.40; N, 8.93.

fac-(4-Dimethylaminopyridine)tricarbonyl(11-(4-dimethylaminophenyl)dipyrido[3,2-a:2′,3′-c]phenazine)rhenium(I) Hexafluorophosphate, [Re($CO)_3$(dppz-$PhNMe_2$)(dmap)]PF_6. Following the general procedure with *fac*-acetonitriletricarbonyl(11-(4-dimethylaminophenyl)dipyrido[3,2-*a*:2′,3′-*c*]phenazine)rhenium(I) hexafluorophosphate (0.120 g, 0.122 mmol), 4-dimethylaminopyridine (0.372 g, 3.04 mmol), and NH_4PF_6 (0.300 g, 1.84 mmol), [$Re(CO)_3$(dppz-$PhNMe_2$)(dmap)]PF_6 was isolated (0.132 g, 95%)

dx.doi.org/10.1021/ic402082m | *Inorg. Chem.* 2014, 53, 1339–1354

as a purple solid. ^{1}H NMR ($CDCl_3$, 400 MHz): δ 10.04−9.99 (m, 2H), 9.51−9.48 (m, 2H), 8.60 (s, 1H), 8.53−8.51 (m, 2H), 8.26−8.22 (m, 2H), 7.97−7.95 (m, 2H), 7.82−7.80 (m, 1H), 7.66−7.63 (m, 2H), 6.74−6.72 (m, 1H), 6.37−6.34 (m, 2H), 3.20 (s, 6H), 2.86 (s, 6H) ppm. HRMS (ESI) Calcd for $C_{36}H_{29}N_7O_3Re$ ($[M]^+$): m/z 794.1889. Found: 794.1918. Anal. Calcd for $C_{36}H_{29}F_6N_7O_3PRe\cdot H_2O$: C, 45.19; H, 3.27; N, 10.25. Found: C, 44.96; H, 3.55; N, 10.24.

X-ray Crystallography. Crystals were attached with Paratone N to a fiber loop supported in a copper mounting pin, and then quenched in a cold nitrogen stream. Data were collected at 93(1) K using Mo Kα radiation (sealed tube, graphite monochromated) using a Bruker Kappa X8 diffractometer with APEX II detector. The data processing were undertaken with SAINT and XPREP.[58] The crystal of dppz-PhNMe$_2$ was nonmerohedrally twinned with orientation matrices for the two components identified using CELL_NOW.[59] A multiscan absorption correction was applied to the data.[60,61] The structures were solved by direct methods with SHELXS-97, and extended and refined with SHELXL-97.[62,63] The non-hydrogen atoms in the asymmetric unit were modeled with anisotropic displacement parameters and a riding atom model with group displacement parameters used for the hydrogen atoms. X-ray crystallographic data of dppz-PhNPh$_2$ and dppz-PhNMe$_2$ ligands is available in CIF format (Supporting Information). CCDC 953106 and CCDC 953107 contain the supplementary crystallographic data for this Article. These data can be obtained free of charge from The Cambridge Crystallographic Data Centre via www.ccdc.cam.ac.uk/data_request/cif.

Crystal data for dppz-PhNPh$_2$·$CHCl_3$ follow: $C_{37}H_{24}Cl_3N_5$, M = 644.96, orange plate, 0.57 × 0.30 × 0.03 mm^3, triclinic, a = 6.047(2) Å, b = 10.171(2) Å, c = 25.288(6) Å, α = 85.675(9)°, β = 83.516(9)°, γ = 76.627(9)°, V = 1501.5(5) Å^3, space group $P\bar{1}$ (No. 2), Z = 2, μ(Mo Kα) = 0.343 mm^{-1}, $2\theta_{max}$ = 50.12°, 24 095 reflections measured, 5268 independent reflections (R_{int} = 0.0772). The final R1(F) = 0.0501 ($I > 2\sigma(I)$); 0.1048 (all data). The final wR2(F^2) = 0.1006 ($I > 2\sigma(I)$); 0.1199 (all data). GOF = 1.006. CCDC 953106.

Crystal data for dppz-PhNMe$_2$·$CHCl_3$: $C_{27}H_{20}Cl_3N_5$, M = 520.83, orange needle, 0.53 × 0.08 × 0.07 mm^3, triclinic, a = 6.892(1) Å, b = 10.453(2) Å, c = 16.852(2) Å, α = 89.638(7)°, β = 85.067(6)°, γ = 73.619(6)°, V = 1160.3(3) Å^3, space group $P\bar{1}$ (No. 2), Z = 2, μ(Mo Kα) = 0.423 mm^{-1}, $2\theta_{max}$ = 50.16°, 23 700 reflections measured, 4047 independent reflections (R_{int} = 0.0674). The final R1(F) = 0.0614 ($I > 2\sigma(I)$); 0.0955 (all data). The final wR2(F^2) = 0.1296 ($I > 2\sigma(I)$); 0.1484 (all data). GOF = 1.060. CCDC 953107.

Physical Measurements. Aldrich spectroscopic grade or HPLC grade solvents were used for all spectroscopic measurements.

^{1}H NMR spectra were recorded at either 400 MHz on a Varian 400MR spectrometer or at 500 MHz on a Varian 500AR spectrometer. ^{13}C NMR spectra were recorded at 125 MHz on a Varian 500AR spectrometer. All samples were recorded at 25 °C in 5 mm diameter tubes. Chemical shifts were referenced internally to residual non-perdeuterated solvent using δ values as reported by Gottlieb et al.[64]

Electrospray ionization high resolution mass spectra were recorded on a Bruker MicroTOF-Q mass spectrometer operating in positive mode.

Analysis of elemental composition was made by the Campbell Microanalytical Laboratory at the University of Otago, Dunedin, New Zealand, using a Carlo Erba 1108 CHNS combustion analyzer. The estimated error in the measurements is ±0.3%.

Electrochemistry and Spectroelectrochemistry. The electrochemical cell for cyclic voltammetry was made up of a 1 mm diameter platinum rod working electrode embedded in a KeL-F cylinder with a platinum auxiliary electrode and a Ag/AgCl reference electrode. The potential of the cell was controlled by an EG&G PAR 273 A potentiostat with model 270 software. Solutions were typically about 10^{-3} M in CH_2Cl_2 and CH_3CN with 0.1 M tetrabutylammonium hexafluorophosphate (Bu_4NPF_6) as supporting electrolyte, and were purged with nitrogen for approximately 5 min prior to measurement. The Bu_4NPF_6 was recrystallized from ethyl acetate and dried under reduced pressure at 70 °C for 10 h, and then kept at 90 °C until use. The scanning speed was 1 V s^{-1}, and the cyclic voltammograms were calibrated against the decamethylferrocenium/decamethylferrocene (Fc*) couple (−0.012 V in CH_2Cl_2, 0.001 V in CH_3CN) and are reported relative to the saturated calomel electrode (SCE) for comparison with other data by subtracting 0.045 V. All IR spectroelectrochemical measurements were performed in an in-house built OTTLE cell which has been described previously.[65] Briefly, the cell comprises two CaF_2 windows sandwiched to give a path length of approximately 200 μm. The working and counter electrodes are pieces of Pt gauze (area approximately 0.25 mm^2). Specific alignment of the cell allows only the measurement of the working electrode gauze. The pseudoreference electrode of the cell is Ag wire. For each measurement the potential was decreased in gradual steps and held at the particular potential until stabilization had been observed, and IR spectra were recorded at each point. All spectra acquired with this setup were recorded with a Nicolet Nexus 380 FTIR spectrometer, fitted with an MCT detector, and recorded at a resolution of 2 cm^{-1}.

Spectroscopy. Steady state absorption spectra were recorded as solutions on a Perkin-Elmer Lambda 950 UV−vis−NIR spectrometer.

FT-Raman spectra were recorded on solid samples at room temperature, using 196−256 scans and 30 mW power, with a spectral resolution of 4 cm^{-1}. A Bruker Equinox IFS-55 interferometer was used with a FRA/106 S attachment and an excitation wavelength of 1064 nm from a Nd:YAG laser source, and was controlled using the Bruker Opus v5.5 software package. Raman photons were detected by a liquid nitrogen cooled Ge diode (D418T).

Resonance Raman spectra were recorded using a previously described setup.[66−69] Solutions were ∼1 mM in spectroscopic grade toluene, CH_2Cl_2, $CHCl_3$, CH_3CN, and dimethylformamide. Excitation wavelengths of 350.7, 356.4, 406.7, and 413.1 nm were obtained from a krypton-ion laser (Innova I-302, Coherent Inc.), 448.0 and 532.0 nm from solid-state diode lasers (CrystaLaser), and 488.0 and 514.5 nm from an argon-ion laser (Innova Sabre, Coherent Inc.). Laser power at the sample was typically 30 mW. The incident beam and collection lens were arranged in a 135° backscattering geometry to reduce loss of Raman intensity by self-absorption. Scattered light was focused by an aperture-matched lens through a narrow-bandpass filter (Ruggate) to remove Rayleigh scattering and a quartz wedge (Spex) to remove polarization bias, and onto the entrance slit (50 μm) of a spectrograph (Acton Research SpectraPro 500i). The collected light was dispersed in the horizontal plane by a 1200 grooves mm^{-1} ruled diffraction grating (blaze wavelength 500 nm). The light was detected by a liquid-nitrogen cooled back-illuminated Spec-10:100B CCD controlled by a ST-133 controller and WinSpec32 (v2.5.8.1) software (Roper Scientific, Princeton Instruments). Calibration was performed using a 1:1 v/v toluene/acetonitrile solution, with Raman peak positions reproducible to ∼1 cm^{-1}. Samples were held in a spinning NMR tube and spectra obtained with a 5 cm^{-1} resolution.

Steady state emission spectra of the ligands were recorded on a Perkin-Elmer LS50B luminescence spectrometer. Steady state emission spectra of the Re complexes were recorded on the same setup as resonance Raman spectra, as previously described,[66−69] with two alterations: first, the removal of the notch filter before dispersion of the photons at the spectrograph, and, second, the use of a 300 grooves mm^{-1} grating. Variable temperature emission spectra were recorded on this same setup, using a TLC50/Edinburgh/E (Quantum Northwest) temperature control system.

Excited-state emission and absorption transients were acquired using a LP920K transient absorption (TA) system (Edinburgh Instruments). Excitation was carried out using pulsed second-harmonic radiation (532 nm) from a Brilliant (Quantel) Nd:YAG laser operating at 1 Hz and, in TA mode, a Xe900 450W xenon arc lamp controlled by an xP900 lamp pulser was used as the probe source. The photons were dispersed using a TMS300-A Czerny−Turner monochromator with a 1800 grooves mm^{-1} grating, recorded on a R928 (Hamamatsu) photomultiplier, and transcribed on a TDS3012C (Tektronix) digital oscilloscope. A TLC50/Edinburgh/E (Quantum Northwest) temperature control system was used. Adjustment of slit width allowed a single point on the wavelength axis to be recorded with a spectral bandwidth of 0.1−18 nm. Fluorescence correction was applied for the transient absorption

Scheme 1. Synthesis of Compounds Presented in This Article (R = Ph, Me; X = H, NMe_2)[a]

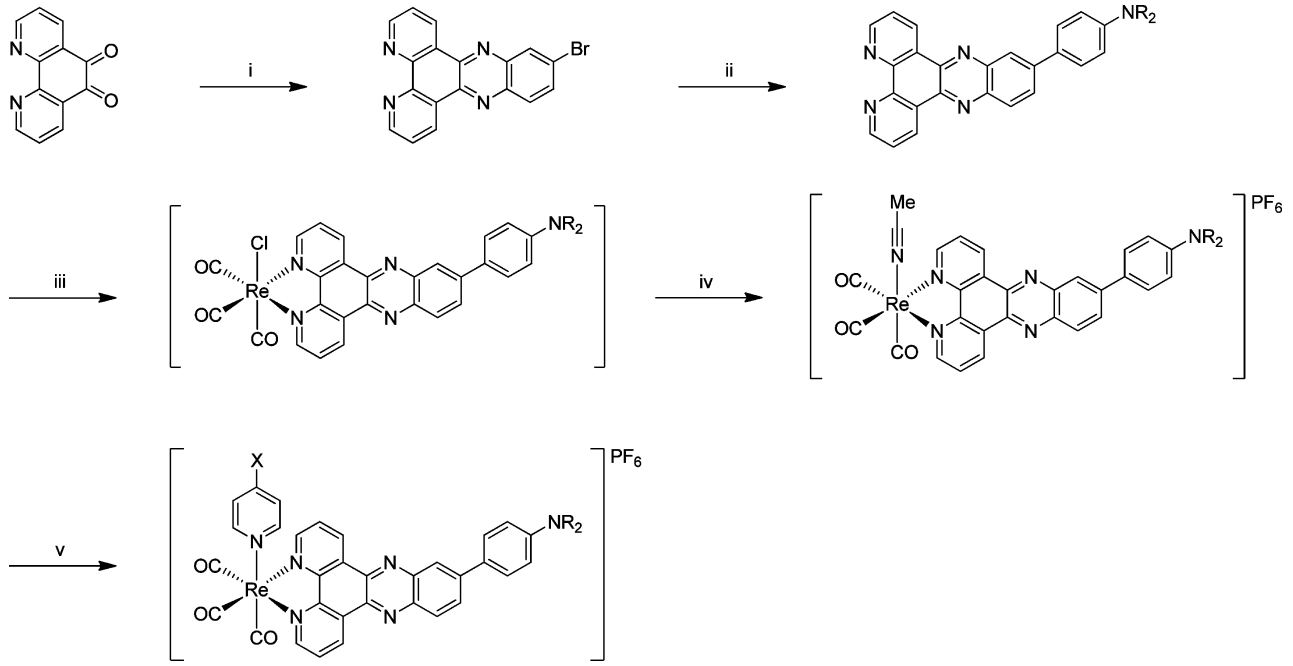

[a]Reaction conditions: (i) 4-bromo-1,2-phenylenediamine, EtOH, room temperature; (ii) 4-(diphenylamino)phenylboronic acid or 4-(dimethylamino)phenylboronic acid, K_2CO_3, $PdCl_2$(dppf), toluene, water, EtOH, reflux; (iii) pentacarbonylrhenium chloride, EtOH, reflux; (iv) AgOTf, CH_3CN, reflux; (v) pyridine or 4-(dimethylamino)pyridine, THF, reflux.

spectra as part of the optical density (ΔOD) calculation. An exponential decay curve was fitted to the output to obtain the lifetime.

TRIR spectroscopy was carried out at the University of Nottingham, on an apparatus that has been described previously.[70,71] Briefly, the output from a commercial Ti:sapphire oscillator (MaiTai)/regenerative amplifier system (Spitfire Pro, Spectra Physics) is split and used to generate 400 nm pump pulses and a tunable mid-IR pulse with a spectral bandwidth of 180 cm^{-1} and a pulse energy of ca. 2 μJ at 2000 cm^{-1}. Half of the IR pulse is reflected onto a single-element mercury cadmium telluride (MCT) detector (Kolmar Technology) to serve as a reference, and the other half serves as the probe beam, which is focused and overlaps with the pump beam at the sample position. The 400 nm pump pulse is optically delayed (up to 3 ns) by a translation stage (LMA Actuator, Aerotech) and focused onto the sample with a quartz lens. The focus spot of the probe beam was adjusted to be slightly smaller than that of the pump beam in order to ensure that the area probed corresponds to excited molecules. The broad-band-transmitted probe pulse is detected with an MCT array detector (Infrared Associates), which consists of 128 elements (1 mm high and 0.25 mm wide). The array detector is mounted in the focal plane of a 250 mm IR spectrograph (DK240, Spectra Product) with a 150 g mm^{-1} grating, resulting in a spectral resolution of *ca.* 4 cm^{-1} at 2000 cm^{-1}. The signals from the array detector elements and the single-element detector are amplified with a 144-channel amplifier and digitized by a 16-bit analogue-to-digital converter (IR-0144, Infrared Systems Development Corp.). A Harrick flowing solution cell with 2 mm thick CaF_2 windows and a path length of 350 μm is mounted on a motorized cell mount that moves the cell rapidly in *x* and *y* dimensions throughout the experiment. Consequently, each laser pulse illuminates a different volume of the sample, reducing heating and degradation of the sample solution.

Spectral data was analyzed using GRAMS A/I (Thermo Scientific) and OriginPro v8.0 (Origin Lab Corporation).

Computational Methods. Calculations were performed using the Gaussian09 package,[72] and calculated spectra generated using GaussSum 2.2.5.[73] DFT calculations utilizing the B3LYP functional were used to optimize the geometry and calculate vibrational frequencies for the lowest energy singlet and triplet states, both *in vacuo* and in a solvent field. Time-dependent DFT calculations (TD-DFT) using the B3LYP and CAM-B3LYP functionals were performed in a solvent field using the polarizable continuum model, implemented using the keyword "scrf" in dichloromethane, chloroform, toluene, and acetonitrile, due to the environmental sensitivity these compounds exhibit. The energy of charge-transfer transitions was underestimated by B3LYP calculations, while this was overestimated by CAM-B3LYP calculations, but to a lesser extent, and therefore spectra were interpreted using CAM-B3LYP calculations. In all calculations, the Re atom was described using the LANL2DZ basis set, while the remaining atoms were described using 6-31G(d). Calculated frequencies were scaled to give the lowest mean absolute deviation (MAD) value. MO models were generated in Gaussview 4.1, and vibrational modes were illustrated using Molden.[74]

The electronic absorption and resonance Raman intensities of the studied compounds were simulated using fitting programs developed by the Myers-Kelley group[75−77] which are based on a time-dependent formulation originally developed by Lee and Heller.[78] The theory involves a consideration of overlap between an excited wavepacket ($|\chi_i(t)\rangle$) propagating along the Franck−Condon surface with the ground state wave function ($|\chi_i\rangle$ when rationalizing the electronic absorption process) and the final wave function ($|\chi_f\rangle$ when rationalizing the resonance Raman intensities). Experimental Raman intensities were corrected for self-absorption, differential bandpass, spectrograph throughput, and detector sensitivity. Band areas were obtained using the peak-fitting module in OriginPro v7.5 (Origin Lab Corporation). The measured solute Raman cross-sections were converted to absolute differential Raman cross sections $(d\sigma_R/d\Omega)_u$ (units $Å^2$ sr^{-1}) by calibration relative to solvent absolute cross-section standards using eq 1

$$\left(\frac{d\sigma_R}{d\Omega}\right)_u = \frac{I_u}{I_v}\frac{c_v}{c_u}\left(\frac{d\sigma_R}{d\Omega}\right)_v \quad (1)$$

where u refers to solute and v to solvent, *I* is the intensity of the peak, and *c* is the concentration. Various solvents were used in this study (CH_2Cl_2, $CHCl_3$, CH_3CN, toluene, DMF), of which the Raman spectra have been previously reported.[68,79−83]

dx.doi.org/10.1021/ic402082m | Inorg. Chem. 2014, 53, 1339−1354

RESULTS AND DISCUSSION

Synthesis. The synthesis of the ligands and complexes is summarized in Scheme 1. The two ligands, dppz-PhNPh$_2$ and dppz-PhNMe$_2$, were prepared by Suzuki–Miyaura palladium-catalyzed cross-coupling between 11-bromodipyridophenazine and an amino-functionalized phenylboronic acid, R$_2$NC$_6$H$_4$B(OH)$_2$ (R = Ph, Me), in yields of 74% and 72%, respectively. Both ligands were isolated as bright orange solids, in contrast to the yellow color characteristic of previously reported dppz ligands.[31,34,38] These two ligands are the first reported examples of diaryl and dialkyl amine-appended dppz systems.

Following previously reported methods for the preparation of [ReCl(CO)$_3$(dppz)] complexes,[34,57] [ReCl(CO)$_3$(dppz-PhNPh$_2$)] and [ReCl(CO)$_3$(dppz-PhNMe$_2$)] were synthesized in yields of 91% and 84%, respectively, as dark solids. Exchange of the chloride ligand for an CH$_3$CN ligand was accomplished by chloride abstraction with AgOTf in CH$_3$CN,[23] to give [Re(CO)$_3$(dppz-PhNPh$_2$)(CH$_3$CN)]PF$_6$ and [ReCl(CO)$_3$(dppz-PhNMe$_2$)(CH$_3$CN)]PF$_6$ in yields of 91% and 86%, respectively. Reaction of these CH$_3$CN complexes with pyridine and 4-(dimethylamino)pyridine yielded [Re(CO)$_3$(dppz-PhNPh$_2$)(py)]PF$_6$ (93%), [Re(CO)$_3$(dppz-PhNPh$_2$)(dmap)]PF$_6$ (93%), [Re(CO)$_3$(dppz-PhNMe$_2$)(py)]PF$_6$ (93%), and [Re(CO)$_3$(dppz-PhNMe$_2$)(dmap)]PF$_6$ (95%).

X-ray crystal structures were obtained for both of the ligands, dppz-PhNPh$_2$ and dppz-PhNMe$_2$ (Figure 3), using a crystal grown from hexane diffusion into a CHCl$_3$ solution in both cases. Both ligands crystallized in the triclinic $P\bar{1}$ space group. The dppz skeleton is virtually planar in both cases, with a maximum deviation from planarity at C18 of 0.171 Å for dppz-PhNPh$_2$ and a maximum deviation at C16 of 0.175 Å for dppz-PhNMe$_2$. For dppz-PhNPh$_2$, the triarylamine adduct is relatively planar, with N5 positioned only 0.053 Å above the plane defined by the *ipso*-carbons of the three aryl substituents (C22, C25, C31). The two triarylamine phenyl groups are rotated from the phenylene linker, with torsion angles of −38.2° and +130.9°. The phenylene linker is rotated −22.8° from the dppz body in dppz-PhNPh$_2$, while only −5.7° in dppz-PhNMe$_2$. As this deviation from coplanarity is only slight in both cases, some retention of conjugation from the dppz to the donor nitrogen is likely. This conjugation pathway manifests itself in the bifurcated hydrogen-bonding of CHCl$_3$ to N1 and N2 of dppz, which is biased toward N2 (from the CHCl$_3$ proton, 2.243 Å to N2 versus 2.515 Å to N1 for dppz-PhNPh$_2$ and 2.252 Å to N2 versus 2.372 Å to N1 for dppz-PhNMe$_2$).

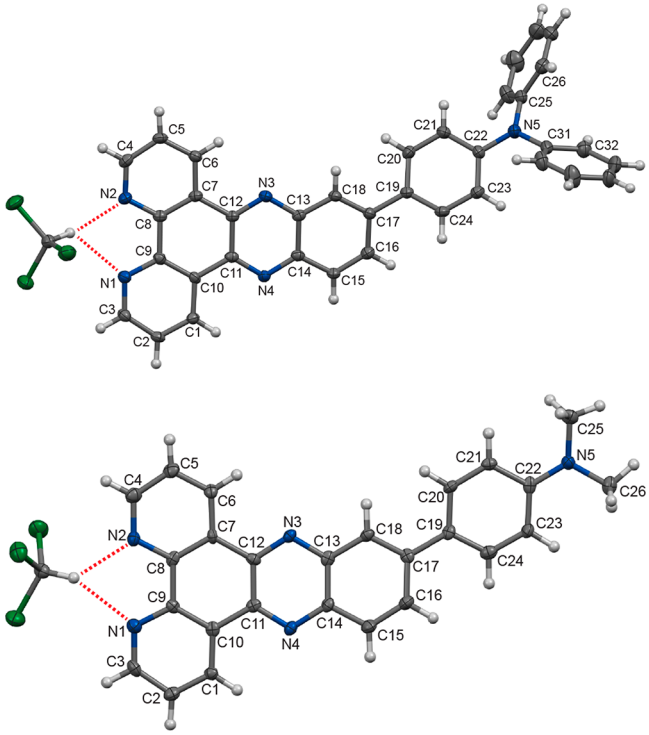

Figure 3. X-ray crystal structures of dppz-PhNPh$_2$ (top) and dppz-PhNMe$_2$ (bottom), both H-bonded with a molecule of CHCl$_3$. Atomic displacement ellipsoids are shown at 50% probability.

The experimental crystallographic data were compared to calculated data. Calculations modeled the rotation of the phenylene linker from the dppz body to be 36.9° for dppz-PhNPh$_2$ and 38.5° for dppz-PhNMe$_2$, overestimated compared to the experimental values. The twist of the two triarylamine phenyl groups from the phenylene linker for dppz-PhNPh$_2$ was calculated with torsion angles of −44.0° and +137.0°, consistent with the experimental results. The greatest difference in bond length between experimental and calculated values is 0.026 Å for dppz-PhNPh$_2$. There is greater deviation in bond length between experimental and calculated values for dppz-PhNMe$_2$, with the largest difference being 0.053 Å. Both of these deviations indicate that there is a good fit between calculated and experimental results.

In order to effectively use the resonance Raman data one can calculate the vibrational frequencies and resulting FT-Raman spectra of the complexes and compare these to the experimental data;[29,40,41,71] in addition to assisting in the band assignments, this is also a test of the reliability of the calculation.[6,31,40,41,84–87] The goodness-of-fit between the experimental and calculated Raman data may be parametrized by the mean absolute deviation (MAD) between the frequencies of the most intense peaks.[40,41,66,71,85,88,89] Figure 4 shows a comparison between the experimental and calculated Raman spectrum for dppz-PhNPh$_2$, which has a MAD of 7 cm^{-1}. The MADs for the other studied compounds range between 5 and 11 cm^{-1}. These are sufficiently small enough to suggest that the calculations adequately model the studied compounds.[40,41,90,91]

Electrochemistry. Electrochemical data for the two ligands and their Re(I) complexes in CH$_2$Cl$_2$ are presented in Table 1. A number of computational and electrochemical studies have indicated that the LUMO in a wide range of dppz ligands and Re(I) complexes is phenazine-based,[1,4,8,33,40,92] on the basis of the observation that the reduction potentials of dppz (−1.28 V vs SCE) occur much closer to that of phenazine (−1.4 V vs SCE) than that of 2,2′-bipyridine (−2.35 V vs SCE).[1] This is further supported by the results obtained from IR spectroelectrochemical measurements. Following reduction of [ReCl(CO)$_3$(dppz-PhNPh$_2$)] (Supporting Information Figure S1) in addition to a shift to lower energy of the ν(CO) bands, several bands were also observed in the 1350–1300 cm^{-1} region of the IR spectrum. The positions of these bands are consistent with the formation of a [phz]$^-$ species.[93] Similar spectral features were observed in the spectra of the [Re(CO)$_3$(dppz-PhNPh$_2$)(dmap)]PF$_6$ and [Re(CO)$_3$(dppz-PhNPh$_2$)(py)]PF$_6$ complexes (Supporting Information Figures S2 and S3). The change in reduction potential is therefore a good indicator of the alteration to the phz MO by the substitution and complexation. Although it is expected that appending

dx.doi.org/10.1021/ic402082m | Inorg. Chem. 2014, 53, 1339–1354

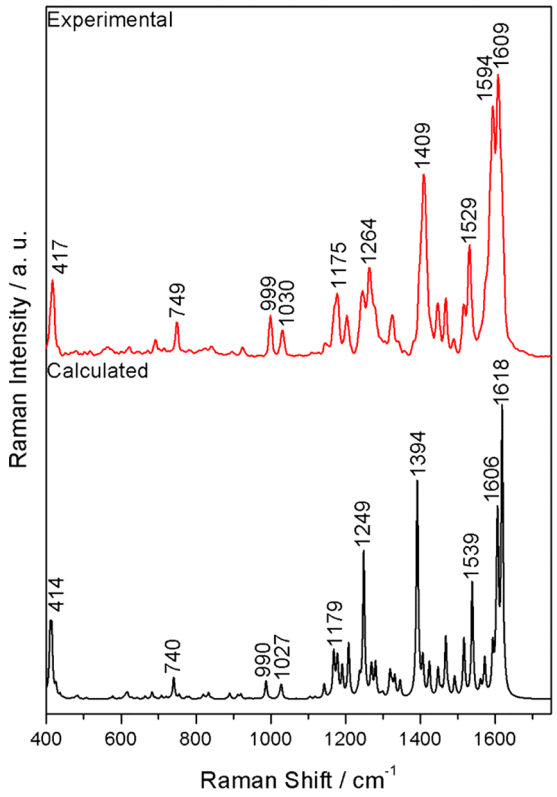

Figure 4. Calculated (black) versus experimental (red) Raman spectra of dppz-PhNPh$_2$.

Table 1. Electrochemical Data for the Ligands and Complexes in CH_2Cl_2

compd	E_{red}[a] (ΔR)[b]/V vs SCE	E_{ox}[a] (ΔR)[b]/V vs SCE
dppz[c]	−1.28	
dppz-PhNPh$_2$	−1.23	1.03
[ReCl(dppz-PhNPh$_2$)(CO)$_3$]	−0.97 (0.26)	1.05 (0.02)
[Re(dppz-PhNPh$_2$)(CO)$_3$(dmap)]PF$_6$	−0.88 (0.35)	1.05 (0.02)
[Re(dppz-PhNPh$_2$)(CO)$_3$py]PF$_6$	−0.85 (0.38)	1.05 (0.02)
dppz-PhNMe$_2$	−1.24	0.91
[ReCl(dppz-PhNMe$_2$)(CO)$_3$]	−1.01 (0.23)	0.95 (0.04)
[Re(dppz-PhNMe$_2$)(CO)$_3$(dmap)]PF$_6$	−0.92 (0.32)	0.96 (0.05)
[Re(dppz-PhNMe$_2$)(CO)$_3$py]PF$_6$	−0.81 (0.43)	1.04 (0.13)

[a] E_{red} and E_{ox} are recorded against $(Fc^*)^+/Fc^*$ and converted to SCE. Solvent CH_2Cl_2, supporting electrolyte Bu_4NPF_6. Irreversible oxidations were observed toward the solvent limit. [b] The change in potential from that of the corresponding ligand. [c] Previously studied,[31] included for comparison.

electron-donating groups to the 11-position of dppz can result in an increase in the reduction potential of the phz MO, a decrease is observed. This was also observed for sulfur-based donor dppz systems by Fraser et al.,[41] who attributed the lowering of the reduction potential to the extension of conjugation of the phz MO. It can also be observed that the ancillary ligand of the Re complexes affects the reduction potential, which lowers in the order Cl > dmap > py. This order is consistent with the π-accepting capabilities of the ancillary ligands, with py being the most capable and Cl the worst π-acceptor. The fact that the Re ancillary ligand affects the reduction potential is unexpected, as phenazine-based orbitals have very little wave function amplitude on the chelating nitrogens. This implies that the segregated orbital model does not necessarily apply to these compounds. As expected, the oxidation potentials of the amine-based donors were similar across the range of compounds, and are consistent with literature values.[43,47,94,95]

In order to probe the solvent interaction of these species, the electrochemical properties of dppz-PhNPh$_2$, [ReCl(CO)$_3$(dppz-PhNPh$_2$)], dppz-PhNMe$_2$, and [ReCl(CO)$_3$(dppz-PhNMe$_2$)] were further investigated in CH_3CN and compared to those in CH_2Cl_2 (Table 2). The reduction

Table 2. Electrochemical Data for the Ligands and $[ReCl(CO)_3(dppz\text{-}Ph\text{-}NR_2)]^{n+}$ (R = Ph, Me) Complexes in CH_2Cl_2 and CH_3CN

	CH_2Cl_2			CH_3CN		
compd	E_{red}/V vs SCE	E_{ox}/V vs SCE	$E_{ox} - E_{red}$	E_{red}/V vs SCE	E_{ox}/V vs SCE	$E_{ox} - E_{red}$
dppz-PhNPh$_2$	−1.23	1.03	2.26	−0.87	1.04	1.91
[ReCl(dppz-PhNPh$_2$)(CO)$_3$]	−0.97	1.05	2.02	−0.81	1.07	1.88
dppz-PhNMe$_2$	−1.24	0.91	2.15	−1.15	0.91	2.06
[ReCl(dppz-PhNMe$_2$)(CO)$_3$]	−1.01	0.95	1.96	−0.77	1.08	1.85

potential (E_{red}) shifts to more positive potentials in CH_3CN; this suggests that the LUMO is decreasing in energy upon increasing solvent polarity. This is further examined using resonance Raman excitation profiles, *vide infra*. The oxidation potential was relatively unaffected upon changing solvent.

Electronic Absorption Spectroscopy. The electronic absorption spectra of dppz-PhNPh$_2$ and its Re(I) complexes are presented in Figure 5. The electronic absorption spectra of the

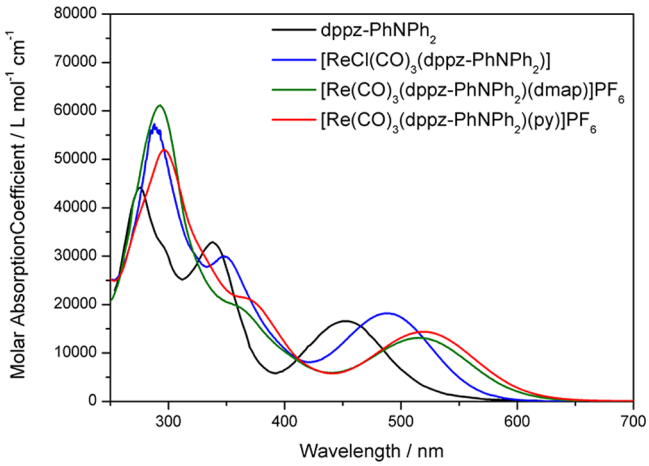

Figure 5. Absorption spectra of dppz-PhNPh$_2$ and [Re(CO)$_3$(dppz-PhNPh$_2$)X]$^{n+}$ (X = Cl, n = 0; X = py, dmap, n = 1) complexes in CH_2Cl_2.

two ligands show a low energy band at 457 nm (dppz-PhNPh$_2$) and 463 nm (dppz-PhNMe$_2$). This band is significantly red-shifted from that of dppz (378 nm). A similar band was observed by Fraser et al. for dppz ligands appended with sulfur-based donors and assigned as an ILCT band.[40] In {Re(CO)$_3$X} systems it is possible to vary the dπ MO energies by the ancillary substituents at X such as py, Cl$^-$, and DMAP.[10] The

dx.doi.org/10.1021/ic402082m | Inorg. Chem. 2014, 53, 1339−1354

Table 3. Experimental and Calculated Electronic Absorption Data and Change in Mulliken Charge Density Calculations

	expt		calcd			Mulliken charge density change (%)			
compd	λ/nm	ϵ/M^{-1} cm^{-1}	λ/nm	f	major MO configuration	metal	Phen	Phz	adduct
dppz-PhNPh$_2$	457	16 900	374	0.84	H-1 → LUMO (18%), HOMO → LUMO (69%)		8 → 23 (15)	16 → 71 (55)	75 → 6 (−69)
[ReCl(CO)$_3$(dppz-PhNPh$_2$)]	492	17 710	399	0.82	H-3 → LUMO (13%), HOMO → LUMO (75%)	0 → 0(0)	2 → 32 (30)	13 → 63 (50)	85 → 5 (−80)
[Re(CO)$_3$(dppz-PhNPh$_2$)(py)]PF$_6$	522	14 400	414	0.76	H-1 → LUMO (12%), HOMO → LUMO (74%)	1 → 2(1)	2 → 43 (41)	11 → 52 (41)	87 → 3 (−84)
[Re(CO)$_3$(dppz-PhNPh$_2$)(dmap)]PF$_6$	519	13 050	421	0.83	H-2 → LUMO (11%), HOMO → LUMO (76%)	0 → 1(1)	2 → 40 (38)	12 → 54 (42)	86 → 4 (−82)
dppz-PhNMe$_2$	463	13 100	373	0.69	H-2 → LUMO (12%), HOMO → LUMO (79%)		8 → 24 (16)	21 → 73 (52)	71 → 3 (−68)
[ReCl(CO)$_3$(dppz-PhNMe$_2$)]	501	12 400	395	0.72	HOMO → LUMO (80%)	0 → 1(1)	4 → 34 (30)	19 → 62 (43)	77 → 3 (−74)
[Re(CO)$_3$(dppz-PhNMe$_2$)(py)]PF$_6$	530	10 600	438	0.7494	HOMO → LUMO (80%)	4 → 1 (−3)	7 → 44 (37)	41 → 52 (11)	49 → 2 (−47)
[Re(CO)$_3$(dppz-PhNMe$_2$)(dmap)]PF$_6$	518	9600	432	0.75	HOMO → LUMO (81%)	1 → 1(0)	2 → 43 (41)	16 → 52 (36)	81 → 3 (−78)

effect of these substituents is to stabilize the dπ MOs (in the order py, Cl$^-$, and DMAP). The shifting of the intense transition at 450 nm for [ReCl(CO)$_3$(dppz-PhNPh$_2$)] on going to X = py or DMAP is not consistent with an MLCT band (Figure 5). The experimentally observed shifts in wavelength and relative absorption intensity are correctly predicted by TDDFT (Table 3).

For all of the studied compounds, CAM-B3LYP TD-DFT calculations predicted the charge-transfer band to be predominantly HOMO → LUMO, where the HOMO is mostly localized on the donor moiety and the LUMO is largely phenazine-based (Figure 6). Unlike the charge-transfer

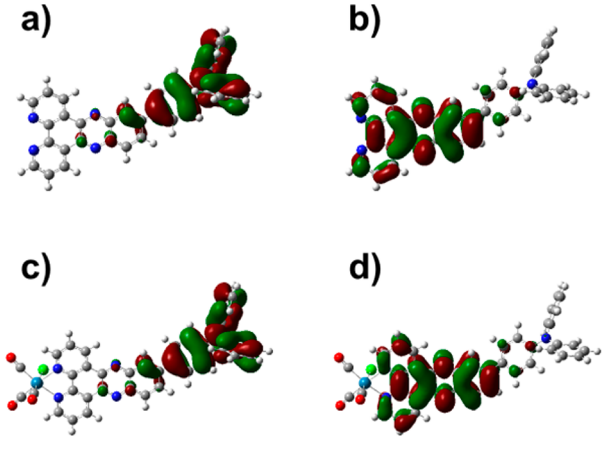

Figure 6. (a) dppz-PhNPh$_2$ HOMO, (b) dppz-PhNPh$_2$ LUMO, (c) [ReCl(CO)$_3$(dppz-PhNPh$_2$)] HOMO, and (d) [ReCl(CO)$_3$(dppz-PhNPh$_2$)] LUMO.

observed by Fraser et al.,[40] our calculations predict no MLCT character in the charge-transfer bands of the Re complexes. The ILCT nature of this low-energy band may also be investigated using Mulliken charge density calculations (Table 3), which show the loss of electron density on the donor and gain of electron density on the dppz body as a result of the transition. It is also interesting to note that, for [Re(CO)$_3$(dppz-PhNPh$_2$)(py)]PF$_6$ and [Re(CO)$_3$(dppz-PhNPh$_2$)(dmap)]PF$_6$, which have very similar absorption spectra, the lowest energy transition is predicted to involve approximately 40% of the electron density change to end up on phz, and 40% on phen, while for [ReCl(CO)$_3$(dppz-PhNPh$_2$)], 50% of the electron density change is predicted to terminate on phz, and 30% on phen.

Resonance Raman Spectroscopy. The nature of the Franck−Condon state can be probed by resonance Raman spectroscopy.[29,96,97] Resonance Raman spectroscopy involves excitation of the probed molecule at the wavelength of an electronic transition, which results in an enhancement of vibrational modes that mimic the nature of the electronic excitation.[71,96,98]

The resonance Raman spectra of dppz-PhNPh$_2$ show the strongest enhancement of a band at 1532 cm^{-1}, with no obvious frequency shift across multiple excitation wavelengths. This mode was assigned using TD-DFT calculations as a phenazine-based mode. Interestingly, the dominant enhancement in the resonance Raman spectra of dppz-PhNMe$_2$ ranged from 1539 cm^{-1} at the shortest excitation wavelengths to 1530 cm^{-1} at the longest wavelengths. This mode was assigned as being delocalized over the entire molecule. Both of the ligands show enhancement of phenylene linker and donor group modes (1595 cm^{-1} and 1607 cm^{-1} for dppz-PhNPh$_2$, 1600 cm^{-1} for dppz-PhNMe$_2$) at excitation wavelengths coinciding with the charge-transfer band. This is consistent with the donor group and the dppz body being involved in the electronic transition in the ligands.

All of the complexes have similar band enhancements to that of [ReCl(CO)$_3$(dppz-PhNPh$_2$)] (Figure 7), ranging between 1530 and 1540 cm^{-1}, all of which are assigned as phenazine based, delocalized dppz, or delocalized ligand based modes. The enhancement of phenylene linker and donor-group based modes at ∼1600 cm^{-1} is also observed, while there appears to be only very small enhancement of carbonyl based modes at ∼2040 cm^{-1}, indicating very little influence of the Re in the electronic transitions. The Franck−Condon state appears to be dominated by a single charge-transfer transition from the donor group to dppz. There are only small changes in resonance Raman spectra across a wide excitation wavelength range. TD-DFT calculations predict the lowest energy transition in all compounds as this charge-transfer type from donor to dppz.

Emission Spectroscopy. Solutions of the two ligands are emissive at room temperature. The emission is unaffected by degassing, suggesting it is singlet in origin. The emission data are presented in Table 4. The emission from each ligand was

dx.doi.org/10.1021/ic402082m | Inorg. Chem. 2014, 53, 1339−1354

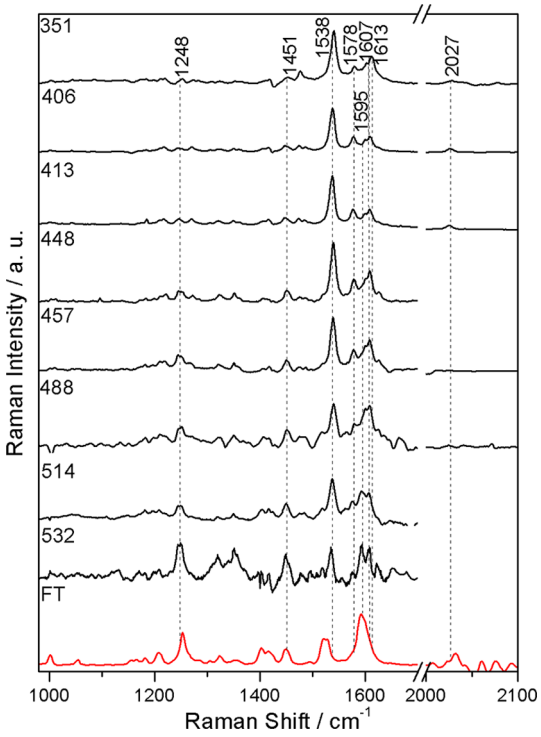

Figure 7. Resonance Raman spectra of $[ReCl(CO)_3(dppz\text{-}PhNPh_2)]$ recorded at various excitation wavelengths for a 1 mM dichloromethane solution. FT-Raman spectrum is shown in red, and was recorded on a solid sample. Solvent bands are denoted with *.

found to be highly solvatochromic. Ligands dppz-$PhNPh_2$ and dppz-$PhNMe_2$ show a variability in the emission wavelengths of 3050 and 2150 cm^{-1}, respectively, upon changing solvent from toluene to CH_2Cl_2. There was no detectable emission in more polar solvents, such as CH_3CN and DMSO, or protic solvents.

The complexes are weakly emissive in a deoxygenated solution, suggesting triplet state emission. Again, no emission was observed in high polarity solvents. The complexes are also solvatochromic, while the coordination of the ligand to rhenium results in a bathochromic shift. The relationship between the Stokes shift and solvent polarity parameter can be related to a change in dipole moment between the ground and emissive excited states through the Lippert−Mataga equation (Figure 8).[99,100] With a fit of the emission data to this model, it was found that the complexes had very similar $\Delta\mu$ to the ligands (~22 D and ~20 D for dppz-$PhNPh_2$ and dppz-$PhNMe_2$, respectively). Despite the ligand emission being attributed to a singlet state and complex emission to a triplet state, they both appear to have similar character, this being ILCT.

The variable-temperature emission spectra of dppz-$PhNPh_2$ in CH_2Cl_2 are presented in Supporting Information Figure S4 and show a blue-shift and increased emission intensity with increasing temperature.

The increase in intensity can be attributed to the emissive state being in thermal equilibrium with a nonemissive (dark) state of lower energy, analogous to the behavior of the molecular light switch, although in this case the nature of these states need not be MLCT.[19] The presence of the dark state is observed in transient absorption spectroscopy, *vide infra*. The dark state has a greater population at low temperature, and the emissive state becomes more thermally populated with increasing temperature. It is important to note that the d−d

Table 4. Absorption and Emission Spectral Data for the Compounds Studied in a Series of Solvents

compd	toluene			dioxane			chloroform			ethylacetate			tetrahydrofuran			dichloromethane			$\Delta\mu$/D
	λ_{abs}/nm	λ_{em}/nm	Stokes shift/cm^{-1}	λ_{abs}/nm	λ_{em}/nm	Stokes shift/cm^{-1}	λ_{abs}/nm	λ_{em}/nm	Stokes shift/cm^{-1}	λ_{abs}/nm	λ_{em}/nm	Stokes shift/cm^{-1}	λ_{abs}/nm	λ_{em}/nm	Stokes shift/cm^{-1}	λ_{abs}/nm	λ_{em}/nm	Stokes shift/cm^{-1}	
dppz-$PhNPh_2$	449	542	3804	443	561	4748	456	620	5788	441	613	6349	447	616	6124	451	653	6847	22
$[ReCl(CO)_3(dppz\text{-}PhNPh_2)]$	488	588	3459	478	626	5911	496	702	6115	473	709	7042	476	709	6907	488	740	6970	25
$[Re(CO)_3(dppz\text{-}PhNPh_2)(dmap)]PF_6$	490	641	4831	479	665	5836	504	717	5904	479	715	6880	491	724	6572	515	721	5534	19
$[Re(CO)_3(dppz\text{-}PhNPh_2)(py)]PF_6$	497	641	4526	485	674	5777	510	727	5881	482	727	6998	492	724	6510	520	783	6459	20
dppz-$PhNMe_2$	454	568	4430	451	597	5447	460	620	5597	453	647	6607	459	656	6531	461	661	6575	20
$[ReCl(CO)_3(dppz\text{-}PhNMe_2)]$	491	640	4751	485	656	5381	500	684	5384	484	735	7051	490	701	6135	500	728	6256	18
$[Re(CO)_3(dppz\text{-}PhNMe_2)(dmap)]PF_6$	492	649	4935	486	657	5351	504	690	5349	*a*	*a*	*a*	600	711	2602	681	817	2455	16
$[Re(CO)_3(dppz\text{-}PhNMe_2)(py)]PF_6$	531	656	3589	494	687	5693	513	710	5403	493	739	6743	508	677	4915	527	752	5682	17

[a]Sample too insoluble to give data.

dx.doi.org/10.1021/ic402082m | *Inorg. Chem.* 2014, 53, 1339−1354

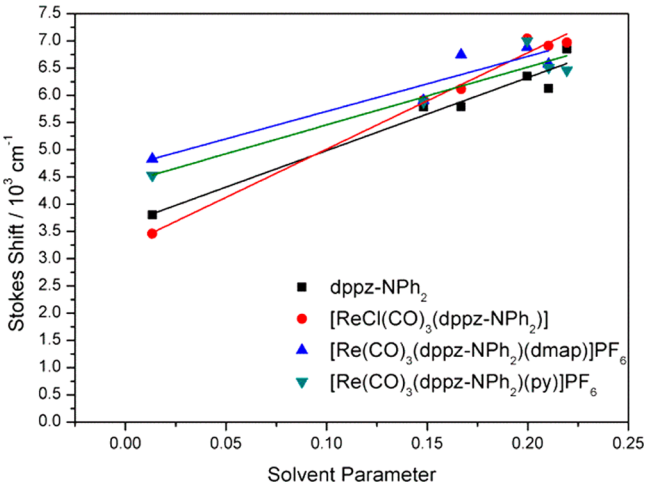

Figure 8. Lippert–Mataga plot for dppz-PhNPh$_2$ and its [Re(CO)$_3$X] complexes.

states that can be occupied in Ru-dppz complexes are too high in energy to be thermally occupied in Re-dppz complexes.[101] Triplet state calculations indicate, for all of the studied compounds, that in the lowest energy triplet state the electronically excited electron occupies a phenazine-based orbital and the positive hole is based on the donor moiety (Supporting Information Table S1). In the segregated orbital model for dppz excited states,[4] the dark state is phenazine-based. This implies that the lowest energy triplet state is the dark state, consistent with the variable-temperature emission spectroscopy. In the optimized geometry of the lowest energy triplet state the phenyl linker group is closer to coplanar relative to the ground state geometry, indicative of extended conjugation in the excited state. This behavior has been previously reported.[102,103]

The temperature-dependent behavior of [ReCl(CO)$_3$(dppz-PhNPh$_2$)] in CH_2Cl_2, and dppz-PhNPh$_2$, dppz-PhNMe$_2$, and [ReCl(CO)$_3$(dppz-PhNMe$_2$)] in toluene, is presented in Supporting Information Figures S5–S8. The increase in emission intensity with increasing temperature is even more pronounced for [ReCl(CO)$_3$(dppz-PhNPh$_2$)] in CH_2Cl_2, indicating a greater separation between the emissive and dark states than dppz-PhNPh$_2$. [ReCl(CO)$_3$(dppz-PhNMe$_2$)] in toluene has a decrease of emission intensity with increasing temperature, indicative of the dark state being higher in energy than the emissive state.

Typically, an increase in temperature results in a bathochromic shift of the emission band because the solvent–fluorophore interaction increases, resulting in a stabilization of the emissive state (and consequent lowering of emission energy).[104,105] However, a slight hypsochromic shift (~150 cm^{-1} over 70 °C) has been observed for the donor–acceptor compound laurdan (6-dodecanoyl-2-dimethylaminonaphthalene) in EtOH.[106] MacGregor and Weber predicted this phenomenon for the donor–acceptor compound prodan (6-propionyl-2-dimethylaminonaphthalene).[107] They identify

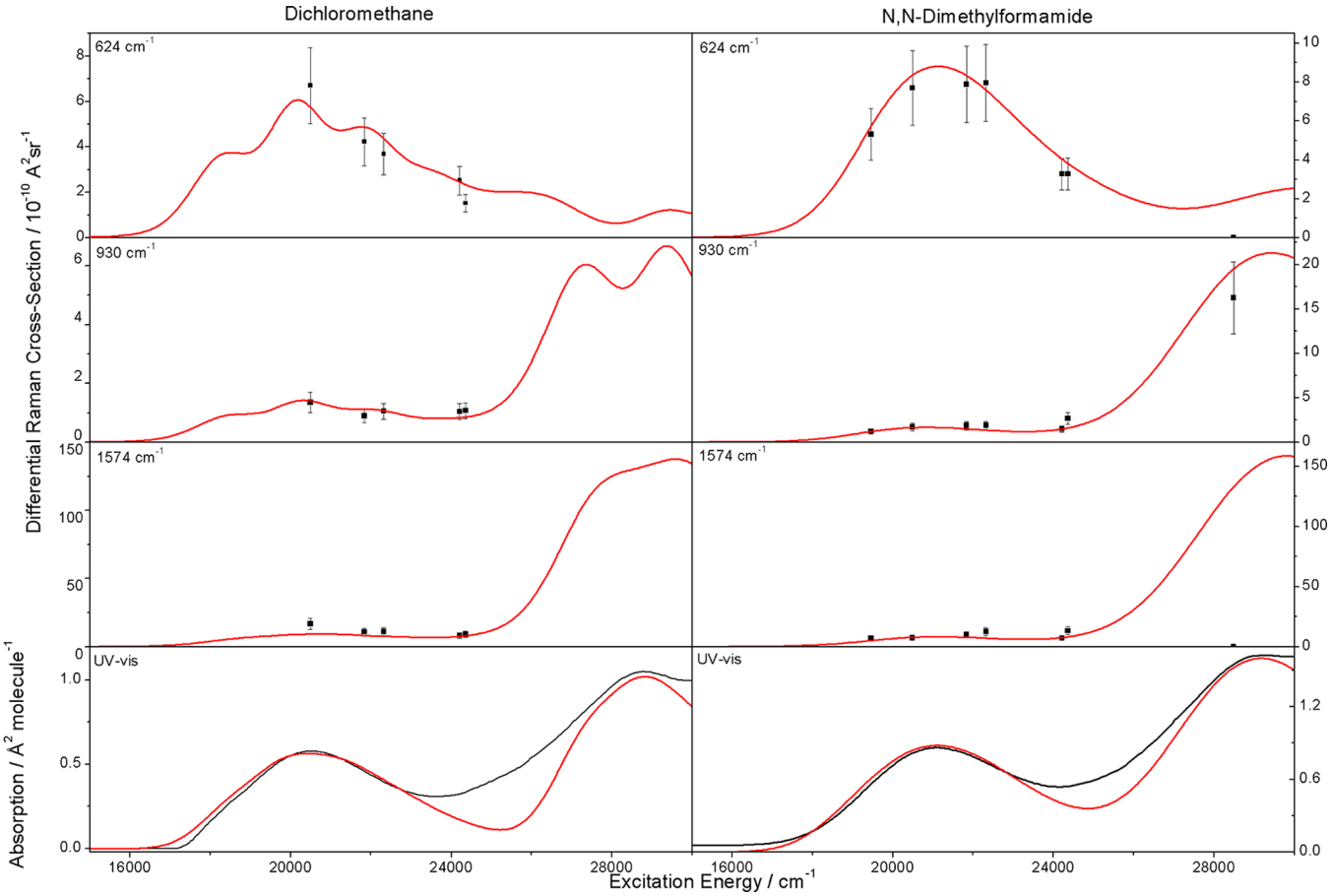

Figure 9. Electronic absorption spectra (fitted red line and experimental black line) and resonance Raman excitation profiles for several vibrational bands (experimental black bars and fits red line) of [ReCl(CO)$_3$(dppz-PhNPh$_2$)] in CH_2Cl_2 and dimethylformamide.

dx.doi.org/10.1021/ic402082m | Inorg. Chem. 2014, 53, 1339–1354

three temperature regimes: (1) a low temperature blue-shift in which the fluorescence lifetime (τ) is significantly less than the correlation time for solvent relaxation (ρ_s); (2) an intermediate temperature red-shift in which τ and ρ_s are of comparable magnitude; (3) a high-temperature blue-shift in which τ is significantly greater than ρ_s. Viard et al. described this same behavior as a maximum stabilization of the emissive state by the solvent at a point where the thermal motion is not able to completely disrupt the orientation of the solvent dipoles, but the solvent is still fluid enough to completely relax before emission occurs.[106] At this stabilization maximum, an increase in temperature increases thermal motion enough to disrupt the orientation of the solvent dipoles, while a decrease in temperature lessens the interaction between solvent and fluorophore due to a decrease in solvent fluidity, in both cases decreasing the stabilization and resulting in a hypsochromic shift.

The ~230 cm^{-1} hypsochromic shift over 40 °C observed in the variable-temperature emission studies of dppz-PhNPh$_2$ in CH_2Cl_2 is more significant than that observed for laurdan (in EtOH). It has been shown that increasing temperature decreases the dielectric constant of a solvent, which in turn decreases the solvent polarity parameter.[108] As the variable-solvent emission studies have shown the studied compounds to be very sensitive to a change in solvent parameter, we propose an analogous model to that of Viard et al.,[106] in which there is competition between the influence of the decreasing dielectric constant of the solvent with increasing temperature and the increased thermal motion of the solvent on the stability of the emissive state. The decreasing solvent dielectric is a destabilizing effect, *vide supra*, and results in a hypsochromic shift, whereas the increasing thermal motion is a stabilizing effect, due to increased interaction between the solvent and the emissive state resulting in a bathochromic shift. According to this model, all of the compounds studied herein appear to be more heavily influenced by the decreasing dielectric constant with increasing temperature.

Resonance Raman Excitation Profiles. The strong solvent-dependence of the emission, coupled with the modest solvatochromism in absorption spectra and the evidence of a number of excited states, encouraged us to examine the absorbing chromophore to investigate the structural distortion of the Franck–Condon (FC) state. The solvent-dependence of the FC states of dppz-PhNPh$_2$, [ReCl(CO)$_3$(dppz-PhNPh$_2$)], dppz-PhNMe$_2$, and [ReCl(CO)$_3$(dppz-PhNMe$_2$)] was investigated using resonance Raman excitation profiles. Absorption spectra and resonance Raman cross sections in toluene, CH_2Cl_2, $CHCl_3$, dimethylformamide, and CH_3CN were modeled using Heller and co-worker's time-dependent wave packet model.[78,109] Resonance Raman excitation profiles for [ReCl(CO)$_3$(dppz-PhNPh$_2$)] are presented in Figure 9, indicating how well the model fits the experimental data.

These analyses provide the structural distortions on going from ground to absorbing state (ΔQ), and this may be related to the reorganization energy (λ). The data are summarized in Table 5 which shows that ΔQ (λ) is larger in DMF and CH_3CN than in toluene, CH_2Cl_2, or $CHCl_3$. This suggests that the energy minimum for the absorbing state is lower in energy in DMF and CH_3CN (Figure 10). If one assumes a ^{1}ILCT absorbing state, then the lowering of its energy would also result in a lower energy ^{3}ILCT state. The transient lifetime and infrared data support the assignment of a long-lived ^{3}ILCT state (*vide infra*). The observation that the compounds are

Table 5. Electronic Parameters Used To Model the Lowest Energy Band of [ReCl(CO)$_3$(dppz-PhNPh$_2$)]

	CH_2Cl_2	$CHCl_3$	Toluene	DMF	CH_3CN
electronic origin (E_{00})/ cm^{-1}	17 050	15 800	17 900	16 700	14 800
homogeneous broadening (Γ_o)/cm^{-1}	1800	2150	2000	2300	3900
electronic dipole length (μ)/Å	1.46	1.36	1.4	1.79	1.03
classical reorganization energy (λ_s)/cm^{-1}	1467	2092	1811	2394	6885

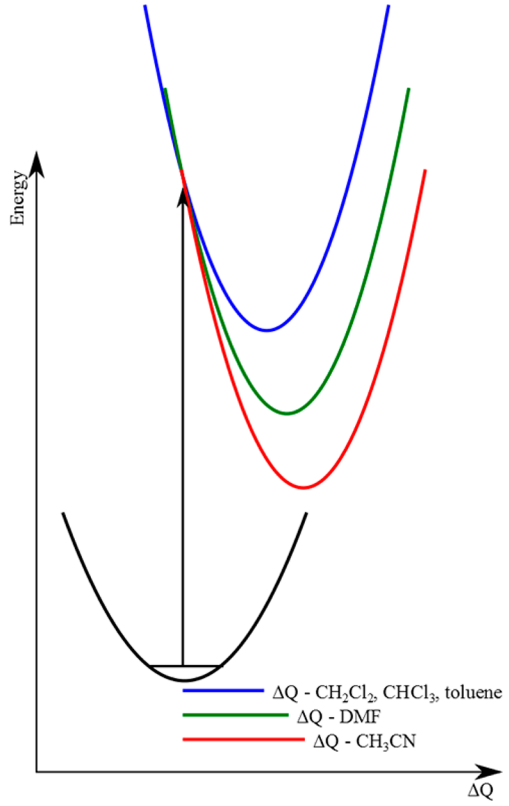

Figure 10. Schematic describing the nature of the Franck–Condon state leading to the observed optical properties.

emissive in CH_2Cl_2 but not in CH_3CN is in accord with the energy gap law.[110] The mode specific data for this compound are presented in Supporting Information Table S5.

Transient Absorption Spectroscopy. The transient absorption data for the two ligands and their complexes are presented in Table 6. Spectral data for [Re(CO)$_3$Cl(dppz-PhNR$_2$)] are shown in Figure 11. All measurements were made with an excitation wavelength of 532 nm. The emissive lifetimes of all compounds were less than 10 ns. For the ligands, no transient absorption measurements were observed at 532 or

Table 6. Transient Absorption Lifetimes (μs) of the Dark States

	dppz-PhNMe$_2$		dppz-PhNPh$_2$	
	CH_2Cl_2	toluene	CH_2Cl_2	toluene
L	<0.01	<0.01	<0.01	<0.01
[ReCl(CO)$_3$(L)]	2.2	6.1	3.8	1.4
[Re(CO)$_3$(L)(dmap)]PF$_6$	2.5	1.1	10.1	1.8
[Re(CO)$_3$(L)(py)]PF$_6$	6.2	0.9	1.6	1.8

dx.doi.org/10.1021/ic402082m | Inorg. Chem. 2014, 53, 1339–1354

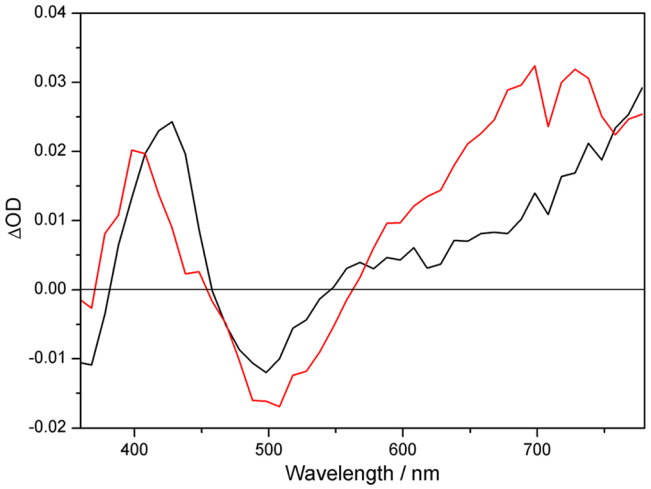

Figure 11. Change in absorption spectra measured for $[Re(CO)_3Cl(dppz\text{-}PhNPh_2)]$ (black line) and $[Re(CO)_3Cl(dppz\text{-}PhNMe_2]$ (red line) in CH_2Cl_2 with 532 nm excitation. Spectra shown are measured 300 ns after excitation. Spectral data for the other complexes are shown in Supporting Information Figure S9.

355 nm. Long-lived excited state TA signals are observed for the complexes.

The transient absorption spectra (358−798 nm) for the complexes show two main features: a strong absorption at ∼400 nm and bleaching of the charge-transfer band (∼450−500 nm). The transient electronic absorption spectra of dppz complexes show similar features. The signal from $[Cu(PPh_3)_2dppz]^{+*}$ shows transient absorption at 460 nm.[34] The absorption profile of $[Re(CO)_3(py)(dppz)]^{+*}$ shows a 460 nm feature with decreasing absorption to the red;[9] very similar features are observed for $[Re(CO)_3(4Mepy)\ (dppz)]^{+*}$.[5] These features are attributed to an IL $\pi\pi^*$ of dppz. The radical anion UV−vis spectrum of dppz has been reported. This shows a distinct band at 584 nm for $[Re(CO)_3Cl(dppz)]^{\bullet-}$ and 587 nm for $[Cu(PPh_3)_2(dppz)]^{\bullet-}$.[92] In our data the appearance of a band at approximately 400 nm provides little detailed information on the excited state nature. However, the observation of absorption bands at $\lambda > 600$ nm is atypical of dppz systems. Such an absorption, at longer wavelengths, is not inconsistent with oxidation of the donor moiety. For example, the radical cation of tris(4-chlorophenyl)amine ($TPACl_3^{\bullet+}$) shows bands at 590 and 680 nm[111] and, for tris(4-bromophenyl)amine ($TPBA^{\bullet+}$), a strong band at 700 nm in MeCN.[112] These data are consistent with the presence of an excited state with ILCT character.

Time-Resolved Infrared Spectroscopy. The carbonyl bands in the infrared may be used to determine the nature of excited states in $\{Re(CO)_3X\}$ systems using time-resolved infrared spectroscopy (TRIR). The backbonding between the $d\pi$ and CO π^* orbitals means that oxidation of the metal, that occurs with MLCT excitation, results in an upshift in frequency $\Delta\nu$. The magnitude of this shift is modulated by backbonding across the $d\pi$ to CO π^* from the ligand π^* MO. Thus, in the case of dppz complexes it is possible to spectroscopically differentiate between MLCT in which the dppz phen MO is populated and that in which the phz MO is populated. Excitation of $[Re(CO)_3(dppzCl_2)(dmap)]^+$ forms a mixture of excited states, one of which is MLCT(phen) in nature. For this state the $\Delta\nu$ = +61 cm^{-1}. For $[Re(CO)_3(dppzCl_2)Cl]$ the excited state is MLCT(phz) in nature and has $\Delta\nu$ = +81 cm^{-1}.

TRIR spectra were measured for $[ReCl(CO)_3(dppz\text{-}PhNPh_2)]$ in CH_2Cl_2, toluene, and CH_3CN, and for $[Re(CO)_3(dppz\text{-}PhNPh_2)(py)]PF_6$ and $[Re(CO)_3(dppz\text{-}PhNPh_2)(dmap)]PF_6$ in CH_2Cl_2. Figure 12 shows the ps-

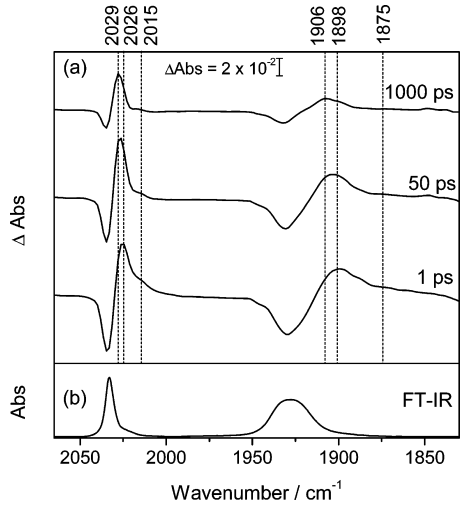

Figure 12. (a) ps-TRIR spectra of $[Re(CO)_3(dppz\text{-}PhNPh_2)(dmap)]PF_6$ in the carbonyl region, at a number of time-delays after photoexcitation with a 400 nm pulse. (b) The FTIR spectrum of $[Re(CO)_3(dppz\text{-}PhNPh_2)(dmap)]PF_6$. Marked peak positions were determined using band-fitting methods.

TRIR spectra of $[Re(CO)_3(dppz\text{-}PhNPh_2)(dmap)]PF_6$ at a number of time-delays, acquired in CH_2Cl_2. Immediately after photoexcitation with a 400 nm pulse, depletion of the parent bands is observed, coincident with the appearance of a new set of red-shifted peaks. Peak-fitting reveals three sets of bands, as summarized in Table 7. A decrease in vibrational frequency

Table 7. IR Stretching Frequencies Observed in CH_2Cl_2 of the Excited States of the Complex $[Re(CO)_3(dppz\text{-}PhNPh_2)(dmap)]PF_6$, after Photoexcitation at 400 nm, and the Ground State FTIR Spectrum

carbonyl stretching frequencies/cm^{-1}	ligand stretching frequencies/cm^{-1}	lifetime/ns (relative amplitude)	state
2034, 1930[a]	1634, 1606, 1591, 1558, 1361, 1335, 1317[a]		GS
2015, 1875		0.020 (0.22)	state I
2026, 1898	1594, 1571, 1331, 1319	0.300 (0.78)	state II
2029, 1906	1600, 1547, 1337, 1307	2800	state III

[a]From FTIR spectrum.

suggests an increased amount of electron density in the carbonyl antibonding orbitals.[10,24,26,113,114] The IR spectrum obtained 1 ps following photolysis shows excited bands at 2026/1898 cm^{-1} and 2015/1875 cm^{-1}. The TRIR reveals the presence of three excited states (I−III), the spectral features of which are presented in Table 7. The shortest lived of these (state I) has bands at 2015 and 1875 cm^{-1}. The decay of this state occurs with the grow in of a long-lived state (III) with features at 2029, 1906, and 1547 cm^{-1}. An additional state (II) with a 300 ps lifetime is observed with bands at 2026, 1898, and 1571 cm^{-1}.

Examination of the CO bands suggests that none of these states have any MLCT character as $\Delta\nu$ (CO) < 0 cm^{-1}. The

dx.doi.org/10.1021/ic402082m | Inorg. Chem. 2014, 53, 1339−1354

CO bands for states II and III are very similar. For the highest frequency CO band $\Delta\nu$ (CO) = −8 and −5 cm^{-1}, respectively. These features may be associated with an intraligand state which may involve the donor moiety. Such shifts have been characterized for other dppz systems with IL(π,π^*) states.[24,26,115,116]

Spectroelectrochemical FTIR on the $[Re(CO)_3Cl(dppz\text{-}PhNPh_2)]^0$ (Supporting Information Figure S1) shows a CO band at 2025 cm^{-1}. As the reduction is phz-based which is the likely acceptor MO in the ILCT transition, this supports the assignment of state II as ILCT. The shifts observed for state III are also consistent with ILCT state, and these data are supported by the transient electronic absorption spectra. The $\Delta\nu$(CO) = −19 cm^{-1} for the highest frequency mode of state I is greater than normally observed for IL states; these features may be due to vibrationally hot states, as have been observed in MLCT states of the TRIR of $[Re(CO)_3(dmap)(dppzNO_2)]^+$.[21] The involvement of the ancillary ligand in the excited state or a breakdown product of the complex may also play a role.[117] State I cannot be unambiguously assigned.

The dynamic behavior of the TRIR suggests the presence of more than one state in the ultrafast time regime. The excited state bands centered at 1898 and 2026 cm^{-1} decay with a lifetime of *ca.* 300 ps concomitant with the partial recovery for the ground state bands. At early times weak bands at 1875 and 2015 cm^{-1} are observed that decay (in 20 ps) to form a new set of peaks at 1906 and 2029 cm^{-1}. The positions of these bands appear unchanged in the ns-TRIR spectra and decay with a lifetime of 2.8 μs which is consistent with the transient absorption data described above given the different concentrations used in these experiments.

The small spectral shift in carbonyl vibrations, between 2026 and 2029 cm^{-1}, coupled with the paucity of the bands at 2015 and 1875 cm^{-1} makes interpretation of these data difficult. Thus, we investigated this further by examining ps-TRIR spectra in the region of ligand-vibrations. Clearer spectral differences exist between spectra in this region, acquired at 50 and 1000 ps, indicating two states of significantly different electronic structures are being probed (Figure 13). The vibrational frequencies are summarized in Table 7. After 1 ps there are two clear peaks at 1571 and 1543 cm^{-1} together with a broad absorption centered around 1325 cm^{-1}. The band at 1571 cm^{-1} together with another band at 1325 cm^{-1} decays (300 ps) at the same rate as the decay of the ν(CO) bands assigned to state II. A band at 1547 cm^{-1} grows within *ca.* 20 ps. The growth of this band is concomitant with the decay of the 2015 cm^{-1} feature (Figure 14). This implies that state I decays as state III appears.

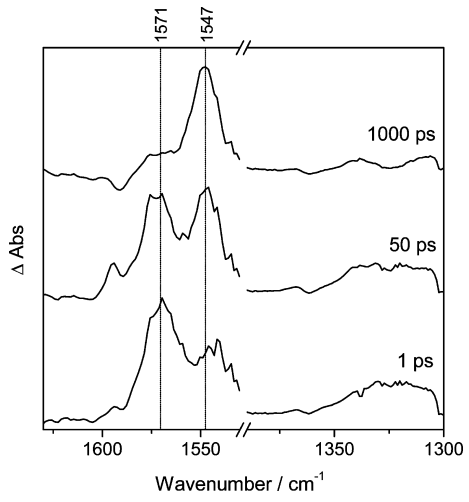

Figure 13. ps-TRIR spectra of $[Re(CO)_3(dppz\text{-}PhNPh_2)(dmap)]PF_6$ in the region of ligand vibrations, at a number of time-delays after photoexcitation with a 400 nm pulse.

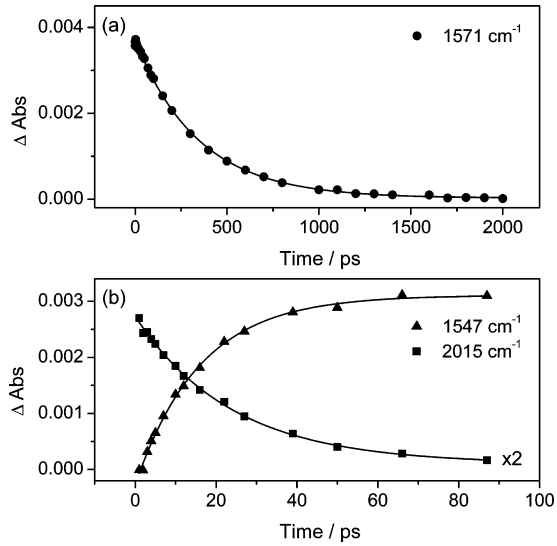

Figure 14. Evolution of prominent features in the ps-TRIR spectra of $[Re(CO)_3(dppz\text{-}PhNPh_2)(dmap)]PF_6$ after photoexcitation with a 400 nm pulse.

These data suggest that states II and III are IL in nature and have charge-transfer character. State I may be due to a vibrationally hot state.

The photophysics of $[ReCl(CO)_3(dppz\text{-}PhNPh_2)]$ has been examined in a range of solvents, and in these experiments, we see the same IR features in the TRIR spectra. In CH_2Cl_2, the parent bands are depleted, and excited-state features are observed with a red-shift of *ca.* 7 cm^{-1} (Supporting Information Figure S10 and Table S3). We observe no evidence for excited-state interconversion. The kinetics of the excited-state absorptions can be fitted to a double exponential with both components being associated with the ligand. No significant solvent-dependent shifts were observed, Supporting Information Table S3. The excited state lifetimes range from 1.6 μs for CH_3CN to 1.2 μs for toluene.

The TRIR spectra of $[Re(CO)_3(dppz\text{-}PhNPh_2)(py)]PF_6$ showed very similar behavior to $[ReCl(CO)_3(dppz\text{-}PhNPh_2)]$, Supporting Information Table S3. TRIR spectroscopy revealed two ligand-centered excited states, which can be assigned as IL states, in accordance with transient absorption, emission, and spectroelectrochemistry measurements. No evidence for MLCT states was observed for any of the complexes, indicating a dominance of the intraligand transitions, consistent with findings from other techniques.

CONCLUSIONS

The synthesis and characterization of two dppz ligands with donor substitution (dppz-Ph-NPh_2 and dppz-Ph-NMe_2) has been reported. The spectral properties of these materials are dominated by very strong ILCT transitions which occur at 450 nm. These transitions shift with complexation to $[Re(CO)_3R]^n$

dx.doi.org/10.1021/ic402082m | *Inorg. Chem.* 2014, 53, 1339−1354

(R = Cl, n = 0; R = py, DMAP, n = +1), but they remain electronically ligand-centered in nature. The MLCT state is not in evidence. The Franck−Condon state has been probed using resonance Raman spectroscopy and TDDFT calculations, and these are consistent with an ILCT transition. The observation of minimal enhancement of the carbonyl bands suggests the MLCT transition contributes very little to the observed optical spectrum.

The ligands are emissive showing strong solvent dependence consistent with an emissive state that has a large dipole moment. Resonance Raman excitation profiles of the complexes, which are not emissive, have been quantified using wavepacket theory. These reveal that the structural distortions between ground and excited states are solvent dependent in a way that is similar to the emissive ligands. Time-resolved infrared studies show spectral shifts in the CO region that support the assignment of ligand-centered excited states. At short time scales there is evidence for three ligand-centered excited states in the observed $\Delta\nu$(CO) band shifts. By using mid-infrared ultrafast spectroscopy the presence of two distinct states is confirmed with bands observed at 1571 and 1547 cm^{-1}, respectively, for each.

■ ASSOCIATED CONTENT

Supporting Information

Figures showing FTIR spectroelectrochemical spectra, variable-temperature emission spectra, transient absorption data, and TRIR data. Tables detailing MOs of the triplet states, resonance Raman excitation profile electronic parameters, TRIR data, *xyz* coordinates for DFT calculations, and resonance Raman cross sections. Crystallographic data in CIF format. This material is available free of charge via the Internet at http://pubs.acs.org.

■ AUTHOR INFORMATION

Corresponding Author

*E-mail: kgordon@chemistry.otago.ac.nz.

Notes

The authors declare no competing financial interest.

■ ACKNOWLEDGMENTS

Support from the University of Otago, The MacDiarmid Institute for Advanced Materials and Nanotechnology, MBIE, and Royal Society of New Zealand is gratefully acknowledged. M.W.G. gratefully acknowledges receipt of a Royal Society Wolfson Merit Award.

■ REFERENCES

(1) Amouyal, E.; Homsi, A.; Chambron, J.-C.; Sauvage, J.-P. *J. Chem. Soc., Dalton Trans.* **1990**, 1841.

(2) Coates, C. G.; Jacquet, L.; McGarvey, J. J.; Bell, S. E. J.; Al-Obaidi, A. H. R.; Kelly, J. M. *J. Am. Chem. Soc.* **1997**, *119*, 7130.

(3) Elias, B.; Creely, C.; Doorley, G. W.; Feeney, M. M.; Moucheron, C.; Kirsch-DeMesmaeker, A.; Dyer, J.; Grills, D. C.; George, M. W.; Matousek, P.; Parker, A. W.; Towrie, M.; Kelly, J. M. *Chem.—Eur. J.* **2008**, *14*, 369.

(4) Fees, J.; Kaim, W.; Moscherosch, M.; Matheis, W.; Klima, J.; Krejcik, M.; Zalis, S. *Inorg. Chem.* **1993**, *32*, 166.

(5) Stoeffler, H. D.; Thornton, N. B.; Temkin, S. L.; Schanze, K. S. *J. Am. Chem. Soc.* **1995**, *117*, 7119.

(6) Lundin, N. J.; Blackman, A. G.; Gordon, K. C.; Officer, D. L. *Angew. Chem., Int. Ed.* **2006**, *45*, 2582.

(7) Klein, A.; Kaim, W.; Waldhor, E.; Hausen, H.-D. *J. Chem. Soc., Perkin Trans. 2* **1995**, 2121.

(8) Atsumi, M.; González, L.; Daniel, C. *J. Photochem. Photobiol., A* **2007**, *190*, 310.

(9) Dyer, J.; Blau, W. J.; Coates, C. G.; Creely, C. M.; Gavey, J. D.; George, M. W.; Grills, D. C.; Hudson, S.; Kelly, J. M.; Matousek, P.; McGarvey, J. J.; McMaster, J.; Parker, A. W.; Towrie, M.; Weinstein, J. A. *Photochem. Photobiol. Sci.* **2003**, *2*, 542.

(10) Kuimova, M. K.; Alsindi, W. Z.; Dyer, J.; Grills, D. C.; Jina, O. S.; Matousek, P.; Parker, A. W.; Portius, P.; Zhong Sun, X.; Towrie, M.; Wilson, C.; Yang, J.; George, M. W. *Dalton Trans.* **2003**, 3996.

(11) Barton, J. *Science* **1986**, *233*, 727.

(12) Broo, A.; Lincoln, P. *Inorg. Chem.* **1997**, *36*, 2544.

(13) Coates, C. G.; Olofsson, J.; Coletti, M.; McGarvey, J. J.; Önfelt, B.; Lincoln, P.; Norden, B.; Tuite, E.; Matousek, P.; Parker, A. W. *J. Phys. Chem. B* **2001**, *105*, 12653.

(14) Olofsson, J.; Önfelt, B.; Lincoln, P.; Nordén, B.; Matousek, P.; Parker, A. W.; Tuite, E. *J. Inorg. Biochem.* **2002**, *91*, 286.

(15) Westerlund, F.; Pierard, F.; Eng, M. P.; Nordén, B.; Lincoln, P. *J. Phys. Chem. B* **2005**, *109*, 17327.

(16) Friedman, A. E.; Chambron, J. C.; Sauvage, J. P.; Turro, N. J.; Barton, J. K. *J. Am. Chem. Soc.* **1990**, *112*, 4960.

(17) Chambron, J.-C.; Sauvage, J.-P. *Chem. Phys. Lett.* **1991**, *182*, 603.

(18) Olson, E. J. C.; Hu, D.; Hormann, A.; Jonkman, A. M.; Arkin, M. R.; Stemp, E. D. A.; Barton, J. K.; Barbara, P. F. *J. Am. Chem. Soc.* **1997**, *119*, 11458.

(19) Brennaman, M. K.; Alstrum-Acevedo, J. H.; Fleming, C. N.; Jang, P.; Meyer, T. J.; Papanikolas, J. M. *J. Am. Chem. Soc.* **2002**, *124*, 15094.

(20) Kuhnt, C.; Karnahl, M.; Tschierlei, S.; Griebenow, K.; Schmitt, M.; Schafer, B.; Krieck, S.; Gorls, H.; Rau, S.; Dietzek, B.; Popp, J. *Phys. Chem. Chem. Phys.* **2010**, *12*, 1357.

(21) Dyer, J.; Grills, D. C.; Matousek, P.; Parker, A. W.; Towrie, M.; Weinstein, J. A.; George, M. W. *Chem. Commun.* **2002**, 872.

(22) Schwalbe, M.; Karnahl, M.; Tschierlei, S.; Uhlemann, U.; Schmitt, M.; Dietzek, B.; Popp, J.; Groake, R.; Vos, J. G.; Rau, S. *Dalton Trans.* **2010**, *39*, 2768.

(23) Dyer, J.; Creely, C. M.; Penedo, J. C.; Grills, D. C.; Hudson, S.; Matousek, P.; Parker, A. W.; Towrie, M.; Kelly, J. M.; George, M. W. *Photochem. Photobiol. Sci.* **2007**, *6*, 741.

(24) Kuimova, M. K.; Sun, X. Z.; Matousek, P.; Grills, D. C.; Parker, A. W.; Towrie, M.; George, M. W. *Photochem. Photobiol. Sci.* **2007**, *6*, 1158.

(25) Kuimova, M. K.; Grills, D. C.; Matousek, P.; Parker, A. W.; Sun, X.-Z.; Towrie, M.; George, M. W. *Vib. Spectrosc.* **2004**, *35*, 219.

(26) Kuimova, M. K.; Alsindi, W. Z.; Blake, A. J.; Davies, E. S.; Lampus, D. J.; Matousek, P.; McMaster, J.; Parker, A. W.; Towrie, M.; Sun, X.-Z.; Wilson, C.; George, M. W. *Inorg. Chem.* **2008**, *47*, 9857.

(27) Arancibia, A.; Concepción, J.; Daire, N.; Leiva, G.; Leiva, A. M.; Loeb, B.; Río, R. D.; Díaz, R.; Francois, A.; Saldivia, M. *J. Coord. Chem.* **2001**, *54*, 323.

(28) David, G.; Walsh, P. J.; Gordon, K. C. *Chem. Phys. Lett.* **2004**, *383*, 292.

(29) Horvath, R.; Gordon, K. C. *Inorg. Chim. Acta* **2011**, *374*, 10.

(30) Kleineweischede, A.; Mattay, J. *J. Organomet. Chem.* **2006**, *691*, 1834.

(31) Lundin, N. J.; Walsh, P. J.; Howell, S. L.; Blackman, A. G.; Gordon, K. C. *Chem.—Eur. J.* **2008**, *14*, 11573.

(32) Lundin, N. J.; Walsh, P. J.; Howell, S. L.; McGarvey, J. J.; Blackman, A. G.; Gordon, K. C. *Inorg. Chem.* **2005**, *44*, 3551.

(33) Walsh, P. J.; Gordon, K. C.; Lundin, N. J.; Blackman, A. G. *J. Phys. Chem. A* **2005**, *109*, 5933.

(34) Waterland, M. R.; Gordon, K. C.; McGarvey, J. J.; Jayaweera, P. M. *J. Chem. Soc., Dalton Trans.* **1998**, 609.

(35) Bolligarla, R.; Das, S. K. *Tetrahedron Lett.* **2011**, *52*, 2496.

(36) Cardinaels, T.; Ramaekers, J.; Driesen, K.; Nockemann, P.; Van Hecke, K.; Van Meervelt, L.; Goderis, B.; Binnemans, K. *Inorg. Chem.* **2009**, *48*, 2490.

(37) Goze, C.; Leiggener, C.; Liu, S.-X.; Sanguinet, L.; Levillain, E.; Hauser, A.; Decurtins, S. *ChemPhysChem* **2007**, *8*, 1504.

(38) Jia, C.; Liu, S.-X.; Tanner, C.; Leiggener, C.; Neels, A.; Sanguinet, L.; Levillain, E.; Leutwyler, S.; Hauser, A.; Decurtins, S. *Chem.—Eur. J.* **2007**, *13*, 3804.
(39) Li, G.-N.; Jin, T.; Sun, L.; Qin, J.; Wen, D.; Zuo, J.-L.; You, X.-Z. *J. Organomet. Chem.* **2011**, *696*, 3076.
(40) Fraser, M. G.; Blackman, A. G.; Irwin, G. I. S.; Easton, C. P.; Gordon, K. C. *Inorg. Chem.* **2010**, *49*, 5180.
(41) Fraser, M. G.; van der Salm, H.; Cameron, S. A.; Barnsley, J. E.; Gordon, K. C. *Polyhedron* **2013**, *52*, 623.
(42) Bronner, C.; Wenger, O. S. *Dalton Trans.* **2011**, *40*, 12409.
(43) Hankache, J.; Niemi, M.; Lemmetyinen, H.; Wenger, O. S. *J. Phys. Chem. A* **2012**, *116*, 8159.
(44) Hankache, J.; Wenger, O. S. *Chem. Commun.* **2011**, *47*, 10145.
(45) Hankache, J.; Wenger, O. S. *Phys. Chem. Chem. Phys.* **2012**, *14*, 2685.
(46) He, B.; Wenger, O. S. *J. Am. Chem. Soc.* **2011**, *133*, 17027.
(47) Mengel, A. K. C.; He, B.; Wenger, O. S. *J. Org. Chem.* **2012**, *77*, 6545.
(48) Reuter, L. G.; Bonn, A. G.; Stückl, A. C.; He, B.; Pati, P. B.; Zade, S. S.; Wenger, O. S. *J. Phys. Chem. A* **2012**, *116*, 7345.
(49) Schmidt, H. C.; Reuter, L. G.; Hamacek, J.; Wenger, O. S. *J. Org. Chem.* **2011**, *76*, 9081.
(50) Wenger, O. S. *Chem. Soc. Rev.* **2012**, *41*, 3772.
(51) Karthikeyan, C. S.; Wietasch, H.; Thelakkat, M. *Adv. Mater.* **2007**, *19*, 1091.
(52) Giribabu, L.; Bessho, T.; Srinivasu, M.; Vijaykumar, C.; Soujanya, Y.; Reddy, V. G.; Reddy, P. Y.; Yum, J.-H.; Gratzel, M.; Nazeeruddin, M. K. *Dalton Trans.* **2011**, *40*, 4497.
(53) Bandara, J.; Willinger, K.; Thelakkat, M. *Phys. Chem. Chem. Phys.* **2011**, *13*, 12906.
(54) Willinger, K.; Fischer, K.; Kisselev, R.; Thelakkat, M. *J. Mater. Chem.* **2009**, *19*, 5364.
(55) Myahkostupov, M.; Castellano, F. N. *Inorg. Chem.* **2011**, *50*, 9714.
(56) Gillard, R. D.; Hill, R. E. E.; Maskill, R. *J. Chem. Soc. A* **1970**, 1447.
(57) Kim, T. Y.; Elliott, A. B. S.; Shaffer, K. J.; John McAdam, C.; Gordon, K. C.; Crowley, J. D. *Polyhedron* **2013**, *52*, 1391.
(58) Area detector control and data integration and reduction software: *SAINT and XPREP*; Bruker AXS Inc.: Madison, WI, 2009.
(59) Program for unit cell determination: Sheldrick, G. M. *CELL_NOW*; University of Göttingen: Göttingen, Germany, 2008.
(60) Scaling for twinned crystals: Bruker AXS Inc.: Madison, WI, 2008.
(61) Empirical absorption correction program for area detector data: Sheldrick, G. M. University of Göttingen: Göttingen, Germany, 2008.
(62) Programs for crystal structure analysis: Sheldrick, G. M. *SHELXS-97 and SHELXL-97*; Göttingen, Germany, 1998.
(63) Sheldrick, G. M. *Acta Crystallogr., Sect. A* **2008**, *64*, 112.
(64) Gottlieb, H. E.; Kotlyar, V.; Nudelman, A. *J. Org. Chem.* **1997**, *62*, 7512.
(65) Krejcik, M.; Danek, M.; Hartl, F. *J. Electroanal. Chem.* **1991**, *317*, 179.
(66) Howell, S. L.; Gordon, K. C. *J. Phys. Chem. A* **2004**, *108*, 2536.
(67) Lind, S. J.; Gordon, K. C.; Waterland, M. R. *J. Raman Spectrosc.* **2008**, *39*, 1556.
(68) Lind, S. J.; Walsh, T. J.; Blackman, A. G.; Polson, M. I. J.; Irwin, G. I. S.; Gordon, K. C. *J. Phys. Chem. A* **2009**, *113*, 3566.
(69) Horvath, R.; Otter, C. A.; Gordon, K. C.; Brodie, A. M.; Ainscough, E. W. *Inorg. Chem.* **2010**, *49*, 4073.
(70) Towrie, M.; Grills, D. C.; Dyer, J.; Weinstein, J. A.; Matousek, P.; Barton, R.; Bailey, P. D.; Subramaniam, N.; Kwok, W. M.; Ma, C. S.; Phillips, D.; Parker, A. W.; George, M. W. *Appl. Spectrosc.* **2003**, *57*, 367.
(71) Fraser, M. G.; Clark, C. A.; Horvath, R.; Lind, S. J.; Blackman, A. G.; Sun, X.-Z.; George, M. W.; Gordon, K. C. *Inorg. Chem.* **2011**, *50*, 6093.
(72) Frisch, M. J.; Trucks, G. W.; Schlegel, H. B.; Scuseria, G. E.; Robb, M. A.; Cheeseman, J. R.; Scalmani, G.; Barone, V.; Mennucci, B.; Petersson, G. A.; Nakasuji, H.; Caricato, M.; Li, X.; Hratchian, H. P.; Izmaylov, A. F.; Bloino, J.; Zheng, G.; Sonnenberg, J. L.; Hada, M.; Ehara, M.; Toyota, K.; Fukuda, R.; Hasegawa, J.; Ishida, M.; Nakajima, T.; Honda, Y.; Kitao, O.; Nakai, H.; Vreven, T.; Montgomery, J. A., Jr.; Peralta, J. E.; Ogliaro, F.; Bearpark, M.; Heyd, J. J.; Brothers, E.; Kudin, K. N.; Staroverov, V. N.; Kobayashi, R.; Normand, J.; Raghavachari, K.; Rendell, A.; Burant, J. C.; Iyengar, S. S.; Tomasi, J.; Cossi, M.; Rega, N.; Millam, N. J.; Klene, M.; Knox, J. E.; Cross, J. B.; Bakken, V.; Adamo, C.; Jaramillo, J.; Gomperts, R.; Stratmann, R. E.; Yazyev, O.; Austin, A. J.; Cammi, R.; Pomelli, C.; Ochterski, J. W.; Martin, R. L.; Morokuma, K.; Zakrzewski, V. G.; Voth, G. A.; Salvador, P.; Dannenberg, J. J.; Dapprich, S.; Daniels, A. D.; Farkas, O.; Foresman, J. B.; Ortiz, J. V.; Cioslowski, J.; Fox, D. J. *Gaussian09*; Gaussian, Inc.: Wallingford, CT, 2009.
(73) O'Boyle, N. M.; Tenderholt, A. L.; Langner, K. M. *J. Comput. Chem.* **2008**, *29*, 839.
(74) Schaftenaar, G.; Noordik, J. H. *J. Comput.-Aided Mol. Des.* **2000**, *14*, 123.
(75) Heller, E. J. *Acc. Chem. Res.* **1981**, *14*, 368.
(76) Shorr, E.; Myers Kelley, A. *Phys. Chem. Chem. Phys.* **2007**, *9*, 4785.
(77) Myers, A. B. *Acc. Chem. Res.* **1997**, *30*, 519.
(78) Lee, S.-Y.; Heller, E. J. *J. Chem. Phys.* **1979**, *71*, 4777.
(79) Moran, A. M.; Kelley, A. M. *J. Chem. Phys.* **2001**, *115*, 912.
(80) Foster, C. E.; Barham, B. P.; Reid, P. J. *J. Chem. Phys.* **2001**, *114*, 8492.
(81) Shoute, L. C. T.; Loppnow, G. R. *J. Am. Chem. Soc.* **2003**, *125*, 15636.
(82) Ziegler, L. D.; Albrecht, A. C. *J. Chem. Phys.* **1979**, *70*, 2634.
(83) Eckhardt, G.; Wagner, W. G. *J. Mol. Spectrosc.* **1966**, *19*, 407.
(84) Cleland, D. M.; Irwin, G.; Wagner, P.; Officer, D. L.; Gordon, K. C. *Chem.—Eur. J.* **2009**, *15*, 3682.
(85) Howell, S. L.; Gordon, K. C.; Waterland, M. R.; Leung, K. H.; Phillips, D. L. *J. Phys. Chem. A* **2006**, *110*, 11194.
(86) Karnahl, M.; Tschierlei, S.; Kuhnt, C.; Dietzek, B.; Schmitt, M.; Popp, J.; Schwalbe, M.; Krieck, S.; Gorls, H.; Heinemann, F. W.; Rau, S. *Dalton Trans.* **2010**, *39*, 2359.
(87) Kuhnt, C.; Tschierlei, S.; Karnahl, M.; Rau, S.; Dietzek, B.; Schmitt, M.; Popp, J. *J. Raman Spectrosc.* **2010**, *41*, 922.
(88) Waterland, M. R.; Howell, S. L.; Gordon, K. C.; Burrell, A. K. *J. Phys. Chem. A* **2005**, *109*, 8826.
(89) Howell, S. L.; Scott, S. M.; Flood, A. H.; Gordon, K. C. *J. Phys. Chem. A* **2005**, *109*, 3745.
(90) Earles, J. C.; Gordon, K. C.; Officer, D. L.; Wagner, P. *J. Phys. Chem. A* **2007**, *111*, 7171.
(91) Clarke, T. M.; Gordon, K. C.; Officer, D. L.; Hall, S. B.; Collis, G. E.; Burrell, A. K. *J. Phys. Chem. A* **2003**, *107*, 11505.
(92) Fees, J.; Ketterle, M.; Klein, A.; Fiedler, J.; Kaim, W. *J. Chem. Soc., Dalton Trans.* **1999**, 2595.
(93) Mattioda, A. L.; Hudgins, D. M.; Bauschlicher, C. W.; Allamandola, L. J.; Bernstein, M.; NavarroGonzalez, R.; Raulin, R. *Space Life Sciences: Astrobiology: Steps toward Origin of Life and Titan before Cassini*; 2005; Vol. *36*, p 156.
(94) Ambrose, J. F.; Carpenter, L. L.; Nelson, R. F. *J. Electrochem. Soc.* **1975**, *122*, 876.
(95) Plater, M. J.; Jackson, T. *Tetrahedron* **2003**, *59*, 4673.
(96) Elliott, A. B. S.; Horvath, R.; Gordon, K. C. *Chem. Soc. Rev.* **2012**, *41*, 1929.
(97) Hirakawa, A. Y.; Tsuboi, M. *Science* **1975**, *188*, 359.
(98) Clark, R. J. H.; Dines, T. J. *Angew. Chem.* **1986**, *98*, 131.
(99) Clarke, T. M.; Gordon, K. C.; Kwok, W. M.; Phillips, D. L.; Officer, D. L. *J. Phys. Chem. A* **2006**, *110*, 7696.
(100) Sakuda, E.; Ando, Y.; Ito, A.; Kitamura, N. *J. Phys. Chem. A* **2010**, *114*, 9144.
(101) Vlček, A., Jr. In *Photophysics of Organometallics*; Lees, A. J., Ed.; Springer: Berlin, 2010; Vol. *29*, p 115.
(102) Damrauer, N. H.; Weldon, B. T.; McCusker, J. K. *J. Phys. Chem. A* **1998**, *102*, 3382.

(103) Meylemans, H. A.; Hewitt, J. T.; Abdelhaq, M.; Vallett, P. J.; Damrauer, N. H. *J. Am. Chem. Soc.* **2010**, *132*, 11464.
(104) Lakowicz, J. R.; Balter, A. *Photochem. Photobiol.* **1982**, *36*, 125.
(105) Weber, G.; Farris, F. J. *Biochemistry* **1979**, *18*, 3075.
(106) Viard, M.; Gallay, J.; Vincent, M.; Meyer, O.; Robert, B.; Paternostre, M. *Biophys. J.* **1997**, *73*, 2221.
(107) Macgregor, R. B.; Weber, G. *Ann. N. Y. Acad. Sci.* **1981**, *366*, 140.
(108) Reish, M. E.; Kay, A. J.; Teshome, A.; Asselberghs, I.; Clays, K.; Gordon, K. C. *J. Phys. Chem. A* **2012**, *116*, 5453.
(109) Tannor, D. J.; Heller, E. J. *J. Chem. Phys.* **1982**, *77*, 202.
(110) Caspar, J. V.; Meyer, T. J. *J. Phys. Chem.* **1983**, *87*, 952.
(111) Amthor, S.; Noller, B.; Lambert, C. *Chem. Phys.* **2005**, *316*, 141.
(112) Wang, R. L.; Tam, K. Y.; Marken, F.; Compton, R. G. *Electroanalysis* **1997**, *9*, 284.
(113) Butler, J. M.; George, M. W.; Schoonover, J. R.; Dattelbaum, D. M.; Meyer, T. J. *Coord. Chem. Rev.* **2007**, *251*, 492.
(114) George, M. W.; Johnson, F. P. A.; Westwell, J. R.; Hodges, P. M.; Turner, J. J. *J. Chem. Soc., Dalton Trans.* **1993**, 2977.
(115) Cao, Q.; Creely, C. M.; Davies, E. S.; Dyer, J.; Easun, T. L.; Grills, D. C.; McGovern, D. A.; McMaster, J.; Pitchford, J.; Smith, J. A.; Sun, X.-Z.; Kelly, J. M.; George, M. W. *Photochem. Photobiol. Sci.* **2011**, *10*, 1355.
(116) Olmon, E. D.; Sontz, P. A.; Blanco-Rodríguez, A. M.; Towrie, M.; Clark, I. P.; Vlček, A.; Barton, J. K. *J. Am. Chem. Soc.* **2011**, *133*, 13718.
(117) Busby, M.; Matousek, P.; Towrie, M.; Vlček, A. *J. Phys. Chem. A* **2005**, *109*, 3000.